Targeted therapy of DC-CIK cells in renal cell carcinoma

Doctoral thesis

to obtain a doctorate (PhD)

from the Faculty of Medicine

of the University of Bonn

Ying Zhang

from Shandong, China

2023

Written with authorization of

the Faculty of Medicine of the University of Bonn

First reviewer: Prof. Dr. Ingo G.H. Schmidt-Wolf

Second reviewer: Prof. Dr. Hans Weiher

Day of oral examination: 20.03.2023

From the Department of Integrated Oncology, CIO Bonn, University Hospital Bonn

Director: Prof. Dr. Ingo G.H. Schmidt-Wolf

Table of Contents

List of Abbreviations

A	
ADCC	antibody-dependent cell-mediated cytotoxicity
APC	antigen-presenting cell
B	
BP	biological process
C	
CC	cell component
CCK-8	cell counting kit-8
chRCC	chromophobe renal cell carcinoma
ccRCC	clear cell renal cell carcinoma
CIK cells	cytokine-induced killer cells
CTLA-4	Cytotoxic T lymphocyte-associated antigen-4
D	
DC	dendritic cell
DEG	differentially expressed gene
F	
FBS	fetal bovine serum
FDA	US Food and Drug Administration
G	
GEO	Gene Expression Omnibus
GM-CSF	granulocyte-macrophage colony-stimulating factor
I	
IRAE	immune-related adverse event
IgG	immunoglobulin gamma
IFN-γ	interferon-γ
IL-1β	interleukin-1β
IL-2	interleukin-2
L	

LFA-1	lymphocyte function-associated antigen 1
M	
MHC	major histocompatibility complex
mTOR	mammalian target of rapamycin
MFI	mean fluorescence intensity
mRCC	meastatic renal cell carcinoma
MF	molecular function
N	
NCBI	National Center for Biotechnology Information
O	
ORR	objective response rates
OS	overall survival
P	
pRCC	papillary renal cell carcinoma
PBMC	peripheral blood mononuclear cell
PD-1	programmed cell death protein 1
PD-L1	programmed cell death protein 1 ligand 1
PFS	progression-free survival
PPI	protein-protein interaction
R	
RCC	renal cell carcinoma
S	
STRING	Search Tool for the Retrieval of Interacting Genes
T	
Treg	regulatory T cells
TKI	tyrosine kinase inhibitor
TNF	tumor necrosis factor
V	
VEGF	vascular endothelial growth factor
VHL	von Hippel-Lindau

7-AAD	7-aminoactinomycin D

1. Introduction

1.1 Renal cell carcinoma

1.1.1 Epidemiology

Kidney cancer accounts for 2.2% of new cases and 1.8% of new deaths for all cancers worldwide (Sung et al., 2021). The incidence of renal cell carcinoma (RCC) in developed countries has doubled over the past half-century, but as more countries are transiting to the Western lifestyle, the global burden is also increasing rapidly.

The epidemiologic characteristics of kidney cancer are large geographic and temporal variations in incidence (Scelo and Larose, 2018). According to the data of GLOBOCAN 2020, Northern America has the highest incidence (age-standardized rate = 12.2/100,000), with Northern Europe (10.3/100,000) and Australia/New Zealand (10.3/100,000) not far behind (https://gco.iarc.fr/today, accessed on 16 August 2022). Lithuania is the country with the highest incidence in the world (14.5/100,000), whereas some nations in Africa and South Asia have an incidence much lower or near 0. The estimated number of deaths is 179,368 reported by GLOBOCAN 2020, with approximately 115,600 men and 63,768 women perishing from the disease in 2020. The cumulative risk of death is 0.28% among men and 0.12% among women worldwide.

The incidence of RCC is increasing by 2% annually during the past two decades worldwide. However, mortality has tended to be stable or decreasing since the 1990s, especially in developed countries. This is partially due to the more frequent physical examination and increased use of abdominal imaging. More than 60% of RCCs are detected incidentally with abdominal imaging, typically with ultrasound, magnetic resonance imaging (MRI), or computed tomography (CT) scan (Ljungberg et al., 2019; Vasudev et al., 2020). The classic triad of flank pain, visible hamaturia, snd a palpable abdominal mass is rare. Even though most of the detected lesions are small renal masses unlikely to be metastasic, locally advanced tumors continue to be diagnosed in a notable number of patients, with distant metastases in ~17% of them (Capitanio and Montorsi, 2016). In general, the survival of patients with RCC depends on the stage when diagnosed. Patients with metastases only have a 12% 5-year survival rate.

The most common age group of diagnosis is between 60 and 70 years old. Those with von Hippel-Lindau (VHL) disease usually develop RCC at an average age of 44 (Maher et al., 2011). As per reports from the SEER database, the median age of patients with RCC was 64 years. Men are predominant in the incidence, with the male-to-female ratio being 1.5:1.

Risk factors for RCC include smoking, obesity, poorly-controlled hypertension, diet, and occupational exposures (Ljungberg et al., 2022; Padala et al., 2020). Smoking is one of the most significant risk factors for RCC (Padala et al., 2020). Continued smoking after RCC diagnosis is also highly associated with worsened overall survival (OS) and progression-free survival (PFS) (Keizman et al., 2014). While heavy drinking is associated with increased risk among men and women, moderate alcohol consumption is associated with a positive effect. Other risk factors for RCC include first-degree relative with RCC, diabetes, draug, and occupational exposure to carcinogens (Tahbaz et al., 2018).

1.1.2 Types

RCC is the most common solid lesion of the kidney that accounts for approximately 90% of all kidney malignancies. RCC comprises a heterogeneous group of subtypes with specific histopathological and genetic characteristics. There are three main RCC types: clear cell RCC (ccRCC), papillary RCC (pRCC), and chromophobe RCC (chRCC) (Hsieh et al., 2017).

Clear cel RCC represents the most common subtype of RCC. 70%-80% of RCCs are ccRCC, and ccRCC accounts for the majority of deaths from kidney cancer. Its histological features include compact nests of tumor cells with clear cytoplasm and architectural patterns such as solid, alveolar, and acinar (Rini et al., 2009). *VHL* gene in ccRCC is the most frequently mutated gene. *VHL* is inactivated by mutation and promoter hypermethylation. Other genetic abnormalitie contains deletions of chromosome 3p segments, gain of chromosome 5q, ans loss of chromosomes 8p, 9p, and 14q. pRCC makes up 10%-15% of all kidney cancers and is divided into two types based on staining features: basophilic (type 1) and eosinophilic (type 2). pRCC contains variable proportions of papillae, tubulopapillae, and tubules. In basophilic pRCC, papillae are lined with one layer of tumor cells with scant pale cytoplasm and low-grade nuclei.

However, eosinophilic pRCC contains abundant eosinophilic cytoplasm and large pseudostratified nuclei with prominent nucleoli. *MET* gene is mutated with gains of chromosomes 7, 8q, 12q, 16p, 17, and 20 and loss of 9p in type 1 pRCC, whereas *CDKN2A*, *SETD2,* and NRF2 are mutated with gains of 8q and loss of 1p and 9p in type 2 pRCC. chRCC only makes up approximately 5% of all kidney tumors. Cells in chRCC are large, polygonal with finely reticulated cytoplasm, distinct cell borders, and atypical nuclei with the perinuclear halo. The tumor cells also have intensely eosinophilic cytoplasm. *TP53* and *PTEN* genes are mutated in chRCC, and loss of chromosomes 1, 2, 6, 10, 13, 17, and 21 are also observed.

Besides the three common RCC subtypes above, additional minor subtypes, including collecting duct carcinoma, clear cell papillary RCC, tubulocystic RCC, and so forth, are also described in the 2022 WHO classification of Tumours of the Urinary System and Male Genital Organs (Moch et al., 2022).

1.1.3 Management

Despite progression in the study of renal cell carcinoma, surgery remains the primary curative treatment. Tumour resection is potentially curative only for patients with the primary tumor in place or single/oligometastatic disease. For these patients, surgery is conducted by either partial or radical nephrectomy with curative intent (Hsieh et al., 2017). However, cytoreductive nephrectomy is palliative for those with inoperable or metastatic disease. For most patients with metastatic RCC (mRCC), systemic treatments with targeted therapy or immunotherapy are necessary.

Several targeted drugs have been approved for the treatment of mRCC in the United States and the European Union. They mainly include inhibitors targeting vascular endothelial growth factor (VEGF) and its receptors (bevacizumab, sunitinib, sorafenib, pazopanib, axitinib, tivozanib, and cabozantinib), and mammalian target of rapamycin (mTOR) pathway inhibition (everolimus and temsirolimus) (Coppin et al., 2011; Hudes, 2009). The VEGFR inhibitor sunitinib and sorafenib have shown significant benefits in PFS and OS compared with placebo in two phase III clinical studies (Escudier et al., 2009; Motzer et al., 2007). In another phase III trial, everolimus prolonged PFS relative

to placebo in patients with mRCC who had progressed after sunitinib or sorafenib treatment (Motzer et al., 2008).

Immune modulators such as interferon α and interleukin-2 were used on mRCC since the 1990s. These agents lead to T-cell-mediated tumour regression and enhance antitumour immune activity. But both agents only show small benefit and are associated with substantial toxicity, especially in the case of high dose IL-2. More studies are now focusing on the new generation of immunotherapy agents, T cell immune checkpoint inhibitors. These include blockade of programmed cell death protein 1 (PD-1) and programmed cell death protein 1 ligand 1 (PD-L1), and CTLA-4. The interaction between PD-1, an inhibitory receptor expressed on lymphocytes and DCs, and PD-L1, the ligand of PD-1 expressed by tumor cells, lead to the down-regulation of the T-cell activity (Massari et al., 2015). PD-1/PD-L1 inhibition promotes T-cell activity and cytotoxicity, and enhance the anti-tumor response. The PD-1 axis inhibitors consist of antibodies against PD-1, including nivolumab and pembrolizumab, and antibodies against (PD-L1), including avelumab and atezolizumab. In 2018, a phase III trial (CheckMate 214) reported a significant benefit of the combination of a PD-1 inhibitor, nivolumab and CTLA-4 inhibitor, ipilimumab over sunitinib. A significantly higher OS and objective response rates (ORR) were achieved on the untreated advanced RCC with nivolumab plus ipilimumab (Motzer et al., 2018).

Cytotoxic T lymphocyte-associated antigen-4 (CTLA-4), a key negative regulator of T cell responses, is the first immune checkpoint to be clinically targeted in oncology (Rudd et al., 2009). CTLA-4 is a type 1 transmembrane glycoprotein of the immunoglobin superfamily and shares 31% amino acid identity with the T cell co-stimulatory receptor, CD28. CTLA-4 and CD28 share the identical ligands: CD80 (B7.1) and CD86 (B7.2) (Azuma et al., 1993; Freeman et al., 1993; Hathcock et al., 1993). When antigen recognition occurs, CD28 and CD80/CD86 interaction promotes TCR signaling to activate T cells. However, CTLA-4 has a higher affinity for both ligands. CTLA-4 can inhibit T cell activity by competing with CD28 for B7 engagement and delivering an inhibitory signal directly from its cytoplasmic tail (Linsley et al., 1994; Riley et al., 2002; Schneider et al., 2006). CTLA-4 functions at the cell surface, but is primarily expressed in the intracellular vesicles (Linsley et al., 1996). Although CTLA-4 is expressed by activated CD8+ effector T cells, its physiological role seems to be mainly

exerted by two major subsets of CD4+ T cells. CTLA-4 engagement results in the inhibition of helper T cell activity and enhancement of regulatory T cells (Tregs) activity (Pardoll, 2012). Ipilimumab is a monoclonal antibody that targets CTLA-4. A phase III trial compared the combination of ipilimumab plus nivolumab with sunitinib for advanced ccRCC. Results showed that the combination achieved significantly higher OS and ORR among intermediate- and poor-risk patients with ccRCC.

However, despite the favorable antitumor response from CTLA-4 blockade, CTLA-4 inhibition also leads to autoimmune manifestations that are referred to as immune-related adverse events (IRAEs) (Barroso-Sousa et al., 2018). One of the most common IRAEs reported clinically is autoimmune thyroid dysfunction. It includes hypothyroidism and hyperthyroidism and is described at potentially high risk after checkpoint inhibitor treatment (Byun et al., 2017; Morganstein et al., 2017). Autoimmune thyroid dysfunction is either caused by primary thyroid gland disorders, or as a result of pituitary dysfunction induced by immune checkpoint blockade (Postow, 2015). The symptoms such as pain, periorbital swelling, or tachycardia have a considerable negative influence on the quality of life of patients who are suffering from cancer (Min et al., 2011). Therefore, it is important to identify the molecule targets and proper strategies to diagnose and manage autoimmune thyroid dysfunction after anti-CTLA-4 therapy.

CD40 is a member of the tumor necrosis factor (TNF) receptor superfamily. CD40 and its ligand CD40L represent one of the most critical molecular pairs of stimulatory immune checkpoints. CD40 is a type I membrane glycoprotein with a cytoplasmic tail, a transmembrane domain, and an extracellular domain on cells. CD40 is widely expressed in various types of cells, such as B cells, DCs, monocytes, and endothelial cells (Banchereau et al., 1994). CD40/CD40L signaling is mediated by the recruitment of TRAFs and NF-κB activation and leads to the activation of innate and adaptive immune cells (Tang et al., 2021). A preclinical study showed that an agonistic anti-CD40 antibody (CP-870,893) stimulated DCs and further promoted the antitumor response of lymph node-derived T cells (Hunter et al., 2007). In a phase I study, the authors also reported that the combination of CP-870,893 and a CTLA-4-blocking mAb (tremelimumab) resulted in T-cell resuscitation and caused tolerable toxicity in patients with metastatic melanoma (Bajor et al., 2018).

1.2 Cytokine-induced killer cells

Cytokine-induced killer (CIK) cells are a cluster of heterogeneous cells comprising CD3+CD56- T cells, CD3-CD56+ NK cells, and CD3+CD56+ NKT cells. Schmidt-Wolf, *et al.* first published the protocol for CIK cell generation in 1991. The increased cytotoxicity of CIK cells against lymphoma and minimal toxicity observed on a SCID mouse/human lymphoma mode was also reported simultaneously (Schmidt-Wolf et al., 1991).

CIK cells can be easily expanded ex vivo from peripheral blood mononuclear cells (PBMCs) (Zhang and Schmidt-Wolf, 2020). 1000 IU/ml of interferon-γ (IFN-γ) should be added on Day 0, and 50 ng/ml monoclonal antibody against CD3 (anti-CD3 mAb), 100 IU/ml interleukin-1β (IL-1β), and 600 IU/ml interleukin-2 (IL-2) should be sequentially added on the next day. IL-2 and fresh culture medium need to be supplemented every 2-3 days for 2-3 weeks. IFN-γ priming 24h before the mitogenic stimulation of anti-CD3 mAb and IL-2 is important, because IFN-γ increases the activation of IL-2-responding cells and activates monocytes to regulate the immunomodulatory factor IL-12 (Bonanno et al., 2010).

CD3+ cells account for over 90% of CIK cells, and the primary effector CD3+CD56+ cells ranged between 7.6% and 65% (Linn et al., 2002). Interestingly, the proportion of the CD3+CD8+ subset increases faster than its CD3+CD56+ counterpart after IL-2 and anti-CD3 stimulation. This CD3+CD56+ population also shows a more terminally differentiated effector phenotype CD27+CD28- or CD27-CD28- than its CD3+CD56− precursors (Linn et al., 2009). CD3+CD56+ cells exert antitumor activity in a major histocompatibility complex (MHC)-unrestricted cytotoxicity against both hematological and solid malignancies.

The decisive molecules and pathways involved in CIK cell cytotoxicity are still under exploration. The natural killer group 2 member D (NKG2D) receptor appears to play the most important role in tumor recognition by CIK cells (Lu et al., 2012). NKG2D is a member of the c-type lectin-activating receptor family identified initially in NK cells, but it is also expressed by activated CD8+ T cells, γδT cells, and NK1.1+ T cells (Jamieson et al., 2002). The ligands of NKG2D consist of MHC class I-related molecules A and B (MIC A/B) and members of the UL16-binding protein family (ULBP1-4), whose

expression are relatively restricted to malignancies. The interaction between NKG2D and its ligands accounts for the majority of the MHC-independent cytotoxicity of CIK cells (Verneris et al., 2004). Besides NKG2D, CIK cells can eradicate tumors in an MHC-restricted manner by TCR engagement(Pievani et al., 2011). Both pathways above could be blocked simultaneously by antibodies against lymphocyte function-associated antigen (LFA-1) and DNAM-1. A preclinical studies also reported that the CD16+ subset of CIK cells could be engaged by trastuzumab or cetuximab and exert potent antitumor response via antibody-dependent cell-mediated cytotoxicity (ADCC) (Cappuzzello et al., 2016).

Many attempts based on CIK cells have been made to achieve higher antitumor activity and more specific recognition against malignancies. To mention, as dendritic cells (DCs) are the most efficient antigen-presenting cells (APCs), the combination of DCs and CIK cells has shown a significant increase in cytotoxic activity (Wang et al., 2010). DCs are a unique APC population that not only initiates antigen-specific immune responses but also regulates immune homeostasis (Balan et al., 2019). DCs capture and process antigens, and present them to the T cells of the immune system. CIK cells combined with DC vaccination compensate for the lack of tumor antigen specificity of CIK cells. In a clinical trial, the autologous tumor lysate-pulsed DC-CIK cell treatment significantly increased the 3-year DFS and decreased the recurrence after surgery in the operable RCC patients (Zhao et al., 2015). Another study based on DC-CIK cell therapy recruited a total of 410 RCC patients after radical or partial nephrectomy, and DC-CIK treatment showed significantly higher benefits on 3- and 5-year OS rates and PFS compared with the IFN-α therapy control group (Zhao et al., 2015).

1.3 High-throughput data analysis

With the progress of high-throughput gene expression profiling technologies, microarrays have provided a valuable method to detect and analyze the expression of thousands of genes simultaneously (Heller, 2002; Townsend et al., 2003). The increasing number of genomic-level data production and bulky raw and processed data files promoted the establishment of high-throughput gene expression databases. Gene Expression Omnibus (GEO) database is one of the international public repositories that archives and freely distributes raw and processed high-throughput data (Clough and

Barrett, 2016). The National Center for Biotechnology Information (NCBI) launched the GEO database in 2000 with the website https://www.ncbi.nlm.nih.gov/geo. Gene data stored in the platform makes it possible to identify differentially expressed genes (DEGs) and find potential biomarkers for human diseases (Kulasingam and Diamandis, 2008).

Another technique that should be emphasized is text mining, also known as Intelligence Text Analysis. Text mining is a powerful tool for automatically extracting information from various written resources by computer (Zhu et al., 2013). Different from web search, the goal of text mining is to discover unknown information from unstructured text. Here we adopted the public tool pubmed2ensembl to perform text mining (http://www.pubmed2ensembl.org). Pubmed2ensembl is an extension of the Ensembl BioMart that integrates large amounts of genomic information from Ensembl and biomedical literature from PubMed (Baran et al., 2011). This tool provides over 2,000,000 links between genes and publications from six curated and automatically generated data sources. It allows us to find a set of functionally related genes based on the relevant literature.

1.4 Purpose of the thesis

Preclinical and clinical studies have shown that CIK cells exhibit promising antitumor efficacy and safety in RCC. Besides, tumor lysate-pulsed DCs combined with CIK cells have shown favorable antitumor response against RCC and other tumors. However, recurrence and non-responsiveness is still a challenging issue for parts of the RCC patients. Considering this, we sought to enhance the antitumor response of DC-CIK cells, presumably as an option for unresponsive patients. To achieve this, we activated DC-CIK cells with anti-CD40 and anti-CTLA-4 antibodies in RCC.

Moreover, although anti-CTLA-4 therapy has provided an effective treatment option for various malignancies such as RCC, the clinical advantages associated with CTLA-4 inhibitors could be offset by the potentially severe immune-related adverse events (IRAEs), including autoimmune thyroid dysfunction. Therefore, it is critical to elucidate the molecular mechanism of autoimmune thyroid dysfunction after anti-CTLA-4 therapy to find practical biological markers and efficient strategies for diagnosing, monitoring, and treating. Here, by bioinformatics, we used microarray data from the

public GEO database to investigate the candidate genes and signaling pathways involved in autoimmune thyroid dysfunction related to anti-CTLA-4 therapy.

In conclusion, the purposes of the thesis are:

1. To investigate the effect of anti-CD40 and anti-CTLA-4 on the antitumor response of DC-CIK cells against RCC;
2. To reveal the candidate genes and signaling pathways involved in autoimmune thyroid dysfunction related to anti-CTLA-4 therapy.

2 Materials and methods

2.1 **Table 1:** Antibodies for flow cytometry

Antibody	**Clone**	**Supplier**
mouse anti-human CD3-FITC	OKT3	BioLegend
mouse anti-human CD8a-Brilliant Violet 421	RPA-T8	BioLegend
mouse anti-human CD56-PE	5.1H11	BioLegend
mouse anti-human CD154-APC	24-31	BioLegend
mouse anti-human CD152-APC	L3D10	BioLegend
mouse anti-human CD28-PerCP/Cyanine5.5	CD28.2	BioLegend
mouse anti-human CD14-FITC	M5E2	BioLegend
mouse anti-human CD16-FITC	3G8	BioLegend
mouse anti-human CD19-FITC	SJ25C1	BioLegend
mouse anti-human CD20-FITC mouse anti-human CD20-FITC	2H7	BioLegend
mouse anti-human CD56-FITC	HCD56	BioLegend
mouse anti-human HLA-DR-PE	L243	BioLegend
mouse anti-human CD11c-PerCP/Cyanine5.5	S-HCL-3	BioLegend

mouse anti-human CD40-APC	5C3	BioLegend
mouse anti-human CD80-APC	2D10	BioLegend
mouse anti-human CD83-APC	HB15e	BioLegend
mouse anti-human CD86-APC	BU63	BioLegend
mouse anti-human CD3-PerCP/Cyanine5.5	OKT3	BioLegend
mouse anti-human CD4-APC	OKT4	BioLegend
mouse anti-human CD25-PE	BC96	BioLegend
mouse anti-human CD127-FITC	A019D5	BioLegend

2.2 Table 2: Antibodies for cell culture and stimulation

Antibody	**Clone**	**Supplier**
anti-human CD40 antibody	G28.5	Bio X Cell
anti-human CD3 antibody	OKT3	eBioscience
human IgG1 isotype control	/	Bio X Cell
ipilimumab (anti-CTLA-4)	monoclonal	Selleckchem
mouse IgG1 isotype control	MOPC-21	Bio X Cell

2.3 Table 3: Chemicals, reagents, and kits

Product	**Supplier**
Annexin V Apoptosis Detection Kit	BioLegend
CFSE	Thermo Fisher Scientific
CCK-8 solution	Dojindo
CellTrace™ Violet dye	Invitrogen

DMSO	Roth
Fixation buffer	Invitrogen
Fetal bovine serum	Gibco
GM-CSF	ImmunoTools
HEPES Buffer	PAN-Biotech
IFN-γ	ImmunoTools
IL-1β	ImmunoTools
IL-2	ImmunoTools
IL-12 p70 Human ELISA Kit	Invitrogen
IFN gamma Human ELISA Kit	Invitrogen
MycoAlert mycoplasma detection kit	Lonza
PBS	Pan-Biotech
Penicillin-Streptomycin	Gibco
Pierce BCA Protein-Assay kit	Thermo Scientific
Permeabilization Buffer	Invitrogen
RPMI-1640	PAN-Biotech
RBC lysis buffer	Biolegend
TNF-α	ImmunoTools
Trypsin-EDTA	Gibco
Zombie Aqua Fixable Viability Kit	BioLegend
7-AAD	Biolegend

2.4 Table 4: Equipments and softwares

Equipments/softwares	**Supplier**
BD FACSCanto II	BD Biosciences
Centrifuge	Thermo Fisher Scientific
Cell culture incubator	Thermo Fisher Scientific
FlowJo v10.6 software	BD Biosciences
GraphPad Prism v.8.0	GraphPad Software
Laminar flow hood	Thermo Fisher Scientific
Multiskan GO Microplate	Thermo Fisher Scientific

Spectrophotometer	
Microscope	ZEISS
RStudio	Posit, PBC
Vortex mixer	Velp Scientifica

2.5 Cell lines

Two human renal carcinoma cell lines Caki-2 and ACHN were purchased from CLS Cell Lines Service GmbH (Eppelheim, Germany). Both were maintained in RPMI-1640 medium supplemented with 10% fetal bovine serum (FBS), 100 U/ml penicillin, and 100 µg/ml streptomycin at 37°C, 5% CO2. Prior to experiments, the cell lines were controlled with MycoAlert mycoplasma detection kit.

2.6 Generation of DCs

Peripheral blood mononuclear cells were isolated from buffy coats of healthy donors (University Hospital Bonn) as previously described (Schmidt-Wolf et al., 1991). As next, PBMCs were set to 5 × 10^6/ml in complete medium (RPMI-1640 medium supplemented with 10% FBS, 100 U/ml penicillin, 100 µg/ml streptomycin, and 2.5% HEPES Buffer 1M) and allowed to adhere to 6-well plates for 3 h, 37°C. Subsequently, we aspirated the medium containing non-adherent cells and washed the plates with warm medium to remove the non-adherent cells. The adherent cells were further cultured with 1000 U/ml GM-CSF and 1000 U/ml IL-4 in complete medium to generate DCs. The medium with necessary cytokines was replaced every 2-3 days. To prepare tumor lysate, ACHN and Caki-2 cells were digested with 0.05% Trypsin-EDTA and washed thrice with PBS. Pelleted cells were resuspended in PBS and lysed via five freeze-thaw cycles. The cell lysate was then centrifuged for 10 min, 13500 g at 4°C. The supernatant was collected and sterilized through a 0.22 µm filter membrane. The protein concentration of the water-soluble tumor lysate was determined using Pierce BCA Protein-Assay kit and stored at −80°C. After six days of culture, the obtained tumor lysate was added to DC culture medium to load DCs at the concentration of 100 µg/ml for 48h. Also,1000 U/ml TNF-α was added to promote maturation for another 24 h.

2.7 DC-CIK cell coculture

CIK cells were generated as previously described (Wu et al., 2020). Briefly, the non-adherent cells achieved above were collected and stimulated by 1000 U/mL IFN-γ for 24 h. On day 1, 50 ng/mL anti-CD3 monoclonal antibody, 600 U/mL IL-2, and 100 U/ml IL-1β were added to continue inducing CIK cells. Cells were then incubated at 37°C in a humidified atmosphere of 5% CO2. Fresh medium with 600 U/mL IL-2 was replenished every 2-3 days. In the ipilimumab or isotype control group, ipilimumab or human IgG1 isotype control was added in CIK cells only once at a concentration of 10 μg/ml at the initiation of culture. After nine days of culture, DCs were collected and cocultured with CIK cells at a ratio of 1:5 in the complete medium supplemented with 600 U/ml IL-2. DC-CIK cells were harvested after 2-3 days for further experiments.

2.8 Phenotype analysis

For phenotype analysis, DCs and CIK cells were washed and resuspended in 100 μl FACS buffer at the concentration of 1×10^7 cells/ml. DCs were stained with PE-HLA-DR, PerCP/Cyanine 5.5-CD11c, APC-CD40, APC-CD80, APC-CD83, APC-CD86, FITC-CD3, FITC-CD14, FITC-CD16, FITC-CD19, FITC-CD20, and FITC-CD56 on ice for 20 min in the dark. For phenotyping of CIK cells, FITC-CD3, Brilliant Violet 421-CD8a, PE-CD56, APC-CD40L, APC-CTLA-4, and PerCP/Cyanine5.5-CD28 were used to stain.

To detect Tregs, the cells were incubated with PerCP/Cyanine5.5-CD3, APC-CD4, Brilliant Violet 421-CD8a, PE-CD25, and FITC-CD127. After two washings, cells were then stained with Zombie Aqua Fixable Viability Kit to exclude dead cells. Samples were acquired on FACSCanto II. Notably, the intracellular expression of CTLA-4 was detected according to the manufacturer's instruction. Briefly, CIK cells were fixed with 100 μl Fixation buffer for 30 min at room temperature. After two subsequent washings by 2 ml 1 × Permeabilization Buffer, cells were resuspended in 100 μl 1 × Permeabilization Buffer and incubated with APC-CTLA-4 for 40 min in the dark. The cells were subsequently washed by 2 ml 1 × Permeabilization Buffer, and 2 ml PBS, and resuspended for analysis.

2.9 Generation of activated T cells

Activated T cells were generated as described by Yano *et al.* (Yano et al., 2014). Briefly, PBMCs were activated with 20 ng/mL anti-CD3 monoclonal antibody and

expanded with 100 U/ml IL-2 in complete medium for 14 days. 10 μg/ml ipilimumab or human IgG1 isotype control was added to CIK cells only once at the initiation of culture.

2.10 Cell counting kit-8 (CCK-8) assay

CCK-8 was performed to test the direct effect of G28.5 and ipilimumab on tumor cells. ACHN (1×10^4 cells/well) and Caki-2 (0.5×10^4 cells/well) cells were incubated with 1 μg/ml, 10 μg/ml, 20 μg/ml, and 40 μg/ml of G28.5 and ipilimumab in 100 μl total volume in 96-well plates. After 24 h of coculture, 10 μl CCK-8 solution was added to each well and incubated with cells for about 3h. The absorbance at 450 nm was measured on Multiskan GO Microplate Spectrophotometer. The viability of tumor cells was calculated using the following formula: Viability = (OD experimental - OD blank)/(OD control − OD blank) × 100%.

2.11 Cytotoxicity assay

The cytotoxicity of DC-CIK cells against RCC cells was detected using flow cytometry, as previously described (Wu et al., 2020). ACHN and Caki-2 cells were labeled by CellTrace™ Violet dye and distributed in 96-well plates at 3×10^4 cells/well and 1.2×10^4 cells/well, respectively. DC-CIK cells, ipilimumab, or hIgG1 treated DC-CIK cells were then cocultured with tumor cells at an E/T ratio of 10:1. After being incubated with 10 μg/ml G28.5 or mIgG1 control for 24 h, all cells were collected, and 7-aminoactinomycin D (7-AAD) was added for live and dead cell discrimination by flow cytometry. The formula used for cytotoxicity calculation is as follows: Cytotoxicity = ((CL − TL)/CL) × 100%. CL, percentage of live tumor cells in control tubes (tumor cells alone); TL, percentage of live tumor cells in test tubes (treatment groups).

2.12 Apoptosis assay

Apoptosis was measured according to the protocol described for FITC Annexin V Apoptosis Detection Kit with 7-AAD. Briefly, the tumor cells were labeled by CellTrace™ Violet dye, and cocultured with DC-CIK cells, ipilimumab, or hIgG1 treated DC-CIK cells at an E/T ratio of 5:1. After incubation with 10 μg/ml G28.5 or mIgG1 control for 10-14 h, all cells were collected and resuspended in 100 μl Annexin V binding buffer. 5 μl FITC Annexin V and 7-AAD were added and incubated at room temperature for 15 min in the

dark. Another 200 μl Annexin V binding buffer was added to each tube, and samples were then analyzed by flow cytometry.

2.13 ELISA assay

The IL-12 secretion of DCs was detected by the IL-12 p70 Human ELISA Kit. First, DCs were distributed at 1 × 10^6 cells/well in 24-well plates in the presence or absence of 10 μg/ml G28.5, ipilimumab, and their isotype controls mIgG1 and hIgG1. After 24h, the supernatant was collected to detect IL-12 secretion by ELISA. The IFN-γ secretion was also detected according to manufacturer's instruction. DC-CIK cells, ipilimumab, or hIgG1 treated DC-CIK cells were cocultured with tumor cells (5 × 10^4 cells/well) at a ratio of 10:1. Subsequently, the cells were incubated with 10 μg/ml G28.5 or mIgG1 control for 24 h. The supernatant was collected to determine the concentration of IFN-γ by the IFN gamma Human ELISA Kit.

2.14 Microarray data

Gene expression profile matrix files of GSE32445 and GSE58062 based on the Illumina MouseWG-6 v2.0 expression beadchip were downloaded from the GEO database (https://www.ncbi.nlm.nih.gov/geo/). The GSE32445 dataset includes five euthyroid and four hypothyroid mouse liver tissue samples, while the GSE58062 dataset contains four euthyroid and four hyperthyroid mouse liver tissue samples.

2.15 Analysis of DEGs

The downloaded matrix TXT files were normalized with the preprocessCore R package (Bolstad, 2019). The DEGs between hypothyroidism or hyperthyroidism and control groups were identified by the empirical Bayes t-test in the Limma R package with |log2 fold change (FC)|>1 and P value < 0.05 set as the threshold values (Durinck et al., 2009; Ritchie et al., 2015). Then the mouse DEGs were converted to their human orthologs in the HGNC symbol by the Biomart package in R (Durinck et al., 2005; Durinck et al., 2009).

2.16 Text mining

The public tool pubmed2ensembl (http://pubmed2ensembl.ls.manchester.ac.uk/) was used to perform text mining. The queries “CTLA-4”, “ipilimumab” and “tremelimumab” were retrieved from up to 100,000 document IDs in the dataset of Homo sapiens genes (GRCh37) filtered in MEDLINE. The common genes from DEGs and text mining were then extracted for the following analysis.

2.17 Gene ontology and pathway enrichment analysis

The GO annotation and KEGG pathway enrichment were performed using the Database for Annotation Visualization and Integrated Discovery (DAVID) (version 6.8) (https://david.ncifcrf.gov/) which offers a series of functional annotation tools to analyze the biological meaning of gene lists systematically. The gene lists achieved above were analyzed with a significance threshold of P value < 0.05.

2.18 Integration of PPI network

We used the online tool STRING (version 11.0) (https://string-db.org/) database to evaluate the relationship between the identified genes above. Only interactions with a combined score > 0.4 were considered to be significant. Cytoscape software (version 3.7.2) was used to analyze and visualize the PPI networks acquired from STRING. The Cytoscape plugin Molecular Complex Detection (MCODE) (version 1.5.1) was used to identify the functional modules within the PPI networks with the following default parameters: Degree Cutoff = 2, Node Score Cutoff = 0.2, K-Core = 2 and Max.Depth = 100. Moreover, to explore key proteins in biological networks, another Cytoscape plugin cytoHubba (version 0.1) was applied to identify the hub genes which rank the top five in all nodes based on the topological analysis method “Degree”.

2.19 Statistical analysis

FACS data sets were analyzed using FlowJo v10.6 software. Statistical analyses were performed using GraphPad Prism v.8.0. Quantitative data are presented as means ± SD. Differences between groups were investigated using Student’s unpaired and paired t-tests, and one-way ANOVA with a Bonferroni correction for multiple comparisons. Each experiment was performed in triplicates and repeated at least three times. $P < 0.05$ was considered statistically significant.

3 Results

3.1 Study 1: Anti-CD40 predominates over anti-CTLA-4 to provide enhanced antitumor response of DC-CIK cells in renal cell carcinoma

3.1.1 Introduction

There is growing interest in CIK cells on the integrated therapy of patients with RCC. Although surgery is still the only curative treatment for localized RCC, for most patients with metastatic disease, systemic therapy, including immunotherapy, is necessarily required (Hsieh et al., 2017). As one of the primary immunotherapy, CIK cells have exhibited promising clinical effects on those patients, but recurrence and non-responsiveness is still a challenging issue. Therefore, several efforts are currently underway to improve the antitumor response of CIK cells.

CIK cells are a cluster of heterogeneous cells comprising CD3+CD56- T cells, CD3-CD56+ NK cells, and CD3+CD56+ NKT cells (Schmidt-Wolf et al., 1993). CIK cells have both non-MHC- restricted cytotoxicity and antitumor activity of T lymphocytes (Introna, 2017). As DCs have a high ability to present tumor antigens and compensate for the lack of tumor antigen specificity of CIK cells, the combination of DCs and CIK cells has shown a significant increase in cytotoxic activity (Wang et al., 2010). CD40 represents one of the most critical stimulatory immune checkpoints. CD40 is a member of TNF receptor superfamily and mainly expressed on B cells, DCs, monocytes, and endothelial cells . A preclinical study reported that CP-870,89 (an agonistic anti-CD40 antibody) stimulated DCs and further promoted the antitumor response of lymph node-derived T cells (Hunter et al., 2007). CTLA-4, another critical immune checkpoint, is also known as a negative regulator of T cells. CTLA-4 is primarily expressed in the intracellular vesicles of T cells and functions by outcompeting CD28 in binding CD80/CD86 on APCs, or enhancing the activity of Tregs (Braun et al., 2021). A phase I study reported that the combination of CP-870,893 and a blocking CTLA-4 mAb tremelimumab resulted in T-cell resuscitation, and increased T-cell activation and tumor T-cell infiltration (Bajor et al., 2018).

Preclinical and clinical studies have shown that CIK cells exhibit promising antitumor efficacy and safety in RCC (Finke et al., 1998; Wang et al., 2014; Zhang et al.,

2012). DCs pulsed with tumor lysate cocultured with CIK cells or activated simultaneously with pembrolizumab (PD-1 inhibitor) have shown favorable antitumor response in RCC patients (Chen et al., 2018; Zhan et al., 2012; Zhao et al., 2015). Considering this, we sought to enhance the antitumor response of DC-CIK cells, presumably as an option for unresponsive patients. We first activated DC-CIK cells with anti-CD40 and anti-CTLA-4 antibodies in RCC cell lines. Then we investigated the cytotoxicity potential, early/late apoptosis levels, and IFN-γ secretion levels. Moreover, we assessed the population of Tregs in CIK cells and highlighted the yet to be known CTLA-4-CD28 interation.

3.1.2 Results

3.1.2.1 Phenotype of CIK cells and DCs

The phenotype of CIK cells and DCs were detected by flow cytometry. The two primary effector subsets of CIK cells, CD3+CD56+ and CD3+CD8+ cells, were significantly increased by 23.2 ± 2.1% and 58.4 ± 12.2% from day 1 to day 14 (Fig. 1a and b). The level of CD40L positive cells was also elevated from 6.0 ± 3.0% to 35.3 ± 5.2% ($P = 0.0011$). To mention, the intracellular CTLA-4 positive cells were significantly decreased from 35.6 ± 2.1% to 4.3 ± 0.8, whereas its counterpart CD28+ cells were also significantly reduced from 62.9 ± 5.0% to 26.57 ± 5.8%. Similarly, Fig. 1b showed that the mean fluorescence intensity (MFI) of CD40L was increased from 671.7 ± 26.5 to 799.3 ± 61.2 ($P = 0.0294$), whereas the MFI of CD28, intracellular and extracellular CTLA-4 were decreased from 5762.0 ± 249.5, 1449.3 ± 47.7, and 744.0 ± 49.4 to 2270.3 ± 136.6 ($P < 0.0001$), 419.7 ± 28.1 ($P < 0.0001$), and 616.0 ± 19.3 ($P = 0.0139$), respectively. As shown in Fig. 1c and d, mature DCs showed significantly increased expression of HLA-DR, CD11c, CD40, CD86, CD80, and CD83 after nine days of culture.

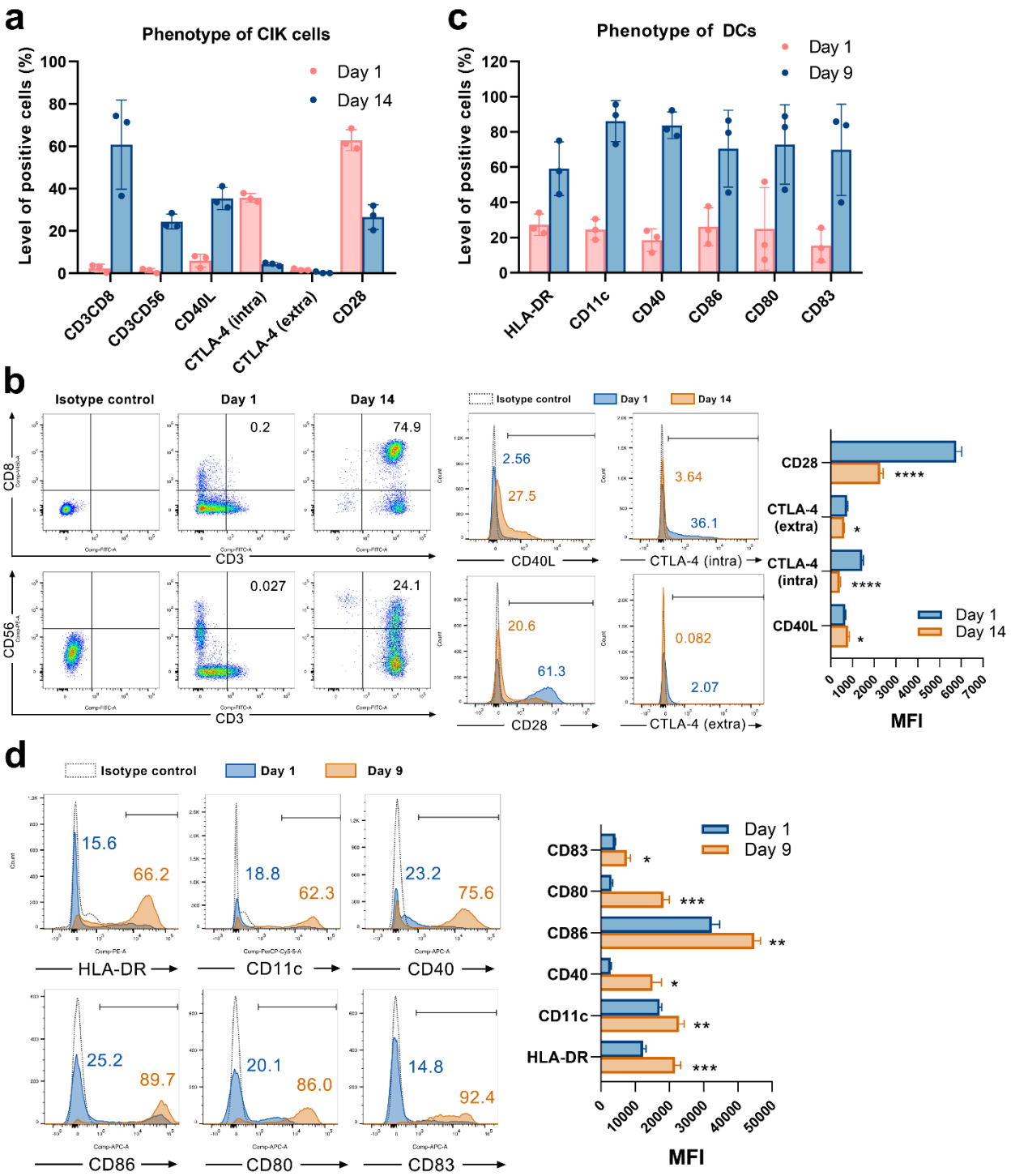

Fig. 1 Characterizing the phenotype of CIK cells and DCs. **a** Phenotype of CIK cells on day 1 and day 14 was detected by flow cytometry. Each bar represents mean ± SD of 3 donors. One representative phenotyping analysis of CIK cells and quantification of the MFI are shown in **b**. **c** The phenotype of DCs on day 1 and day 9 was detected by flow cytometry. Each bar represents mean ± SD of 3 donors. One representative phenotyping analysis of DCs and quantification of the MFI are shown in **d**. Intra: intracellular; extra: extracellular; SD: standard deviation. (* $P < 0.05$, ** $P < 0.01$, *** $P < 0.001$, **** $P < 0.0001$)

3.1.2.2 Anti-CD40 promoted CD3+CD56+ population by DCs

After being incubated with the anti-CD40 antibody (G28.5) for 48 h, DCs showed upregulation of the surface markers CD80, CD83, C86, and HLA-DR, indicating the maturation after anti-CD40 treatment (Fig. 2a and b). Hunter et al. observed similar results when a anti-CD40 antibody (CP-870,893) was used (Hunter et al., 2007). G28.5 IL-12 secretion was also stimulated obviously by 185.6 ± 79.9 pg/ml (P = 0.046) and 204.1 ± 79.9 pg/ml (P = 0.046) in G28.5 and the combination group, individually, which indicates the promoted activation of DCs following G28.5 treatment (Fig. 2c). We further treated DC-CIK and CIK cells with G28.5 to assess any alteration in the CD3+CD56+ effector cells. The increased CD3+CD56+ cells were observed in DC-CIK cells instead of CIK cells alone (P = 0.007) (Fig. 2d). The results show that G28.5 could promote the antitumor response of CIK cells by inducing DC maturation and activation.

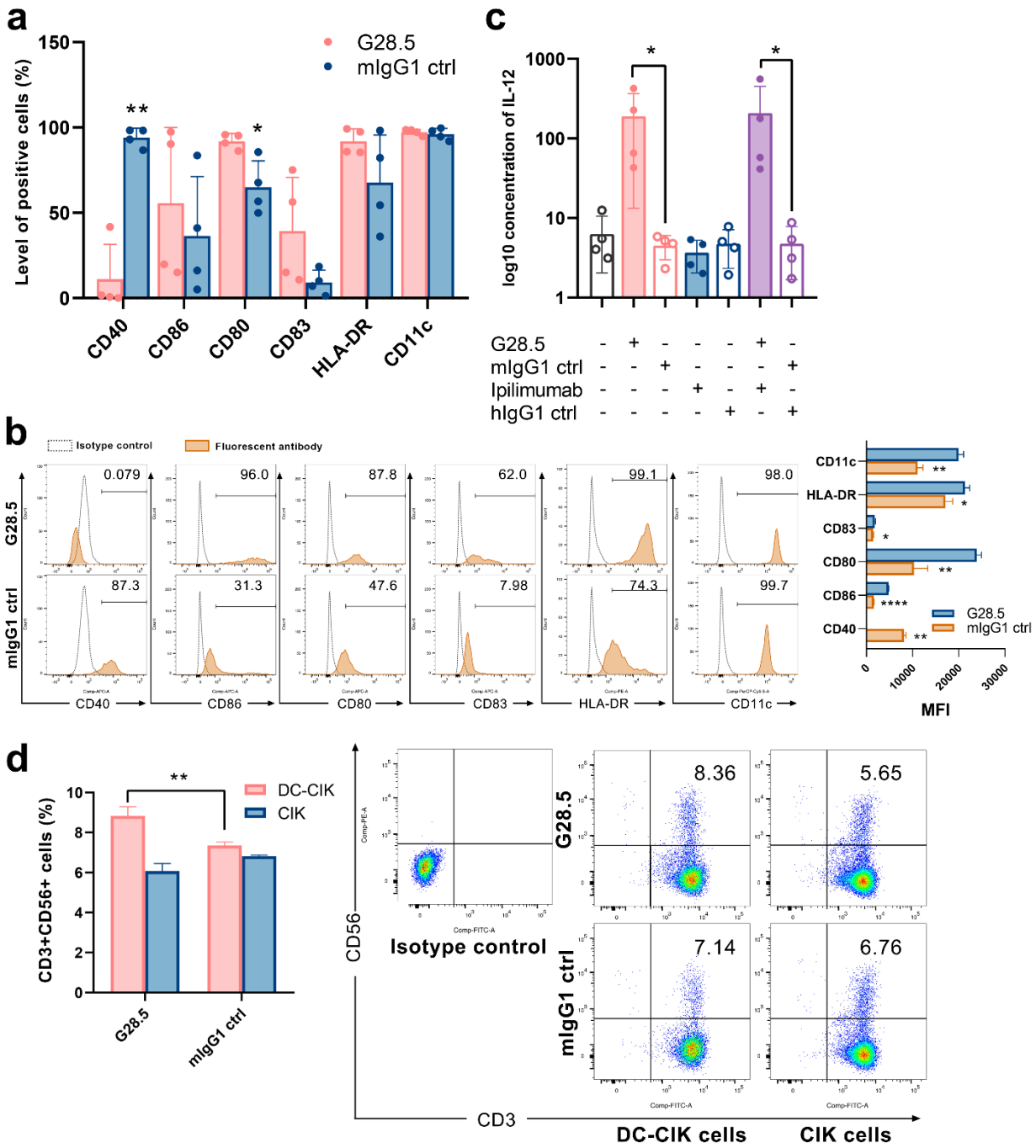

Fig. 2 Anti-CD40 promoted CD3+CD56+ population of CIK cells by inducing DC maturation and activation. **a** The anti-CD40 antibody G28.5 promoted DC mature phenotype. DCs on day 6 were plated at 25 × 10^4 cells/ml in the presence of G28.5 (10 μg/ml) or its isotype control mIgG1 (10 μg/ml) for 48 h. After treatment, phenotypic markers of DCs were detected by flow cytometry. Each bar represents mean ± SD of 4 donors. One representative phenotyping analysis and quantification of the MFI are shown in **b**. **c** G28.5 increased IL-12 secretion of DCs. DCs were distributed at 1 × 10^6 cells/well in 24-well plates in the presence or absence of 10 μg/ml G28.5, ipilimumab, and their isotype controls mIgG1 and hIgG1. After 24 h, the supernatant was collected to detect IL-12 secretion by ELISA. Each bar represents mean ± SD of 4 donors. **d** G28.5

increased the CD3+CD56+ population of CIK cells when cocultured with DCs. CIK cells on day 9 were labeled by CellTrace™ Violet dye and cocultured with DCs at a ratio of 5:1. DC-CIK cells and CIK cells were treated with 10 μg/ml G28.5 or mIgG1 for 48 h. The expression of CD3 and CD56 on CIK cells was measured by flow cytometry. One representative donor (left) and the flow cytometry analysis (right) are shown. (* $P < 0.05$, ** $P < 0.01$, **** $P < 0.0001$)

3.1.2.3 Favorable effects of G28.5 combined with ipilimumab on CTLA-4 expression and CD3+CD56+ effector cells

The effect of G28.5 in combination with ipilimumab (CTLA-4 inhibitor) was next tested on DC-CIK cells. It was observed that G28.5 increased both intracellular and extracellular expression of CTLA-4 by 37.3 ± 0.9% ($P < 0.0001$) and 0.1 ± 0.1% ($P = 0.24$), respectively, in CIK cells when cocultured with DCs, but not in CIK cells alone (Fig. 3a and b). In addition, ipilimumab suppressed the CTLA-4 expression of CIK cells in DC-CIK cells. As CTLA-4 is known as a negative regulator of T cells, it suggested that G28.5 combined with ipilimumab might have a favorable effect on the antitumor response. Moreover, G28.5 and ipilimumab both decreased the expression of CD28 (the counterpart of CTLA-4) in DC-CIK cells. The level of cells positive for CD28 were reduced significantly by 13.5 ± 1.3% by G28.5, by 11.4 ± 0.7% by ipilimumab, and by 24.9 ± 1.2% by the combination in DC-CIK cells (Fig. 3c). Similar to G28.5, ipilimumab increased the CD3+CD56+ population in CIK cells alone (by 1.8 ± 0.2%, $P = 0.001$) or DC-CIK cells (by 1.8 ± 0.4%, $P = 0.006$). The combination of G28.5 and ipilimumab also increased the percentage of CD3+CD56+ cells in DC-CIK cells compared with G28.5 (by 3.8 ± 0.3%, $P < 0.0001$) and ipilimumab (by 0.8 ± 0.3%, $P = 0.3742$) (Fig. 3d). Taken together, we assumed that G28.5 combined with ipilimumab could promote the antitumor response of DC-CIK cells compared to G28 or ipilimumab alone, primarily by reducing inhibitory CTLA-4 and proliferating CD3+CD56+ effector cells.

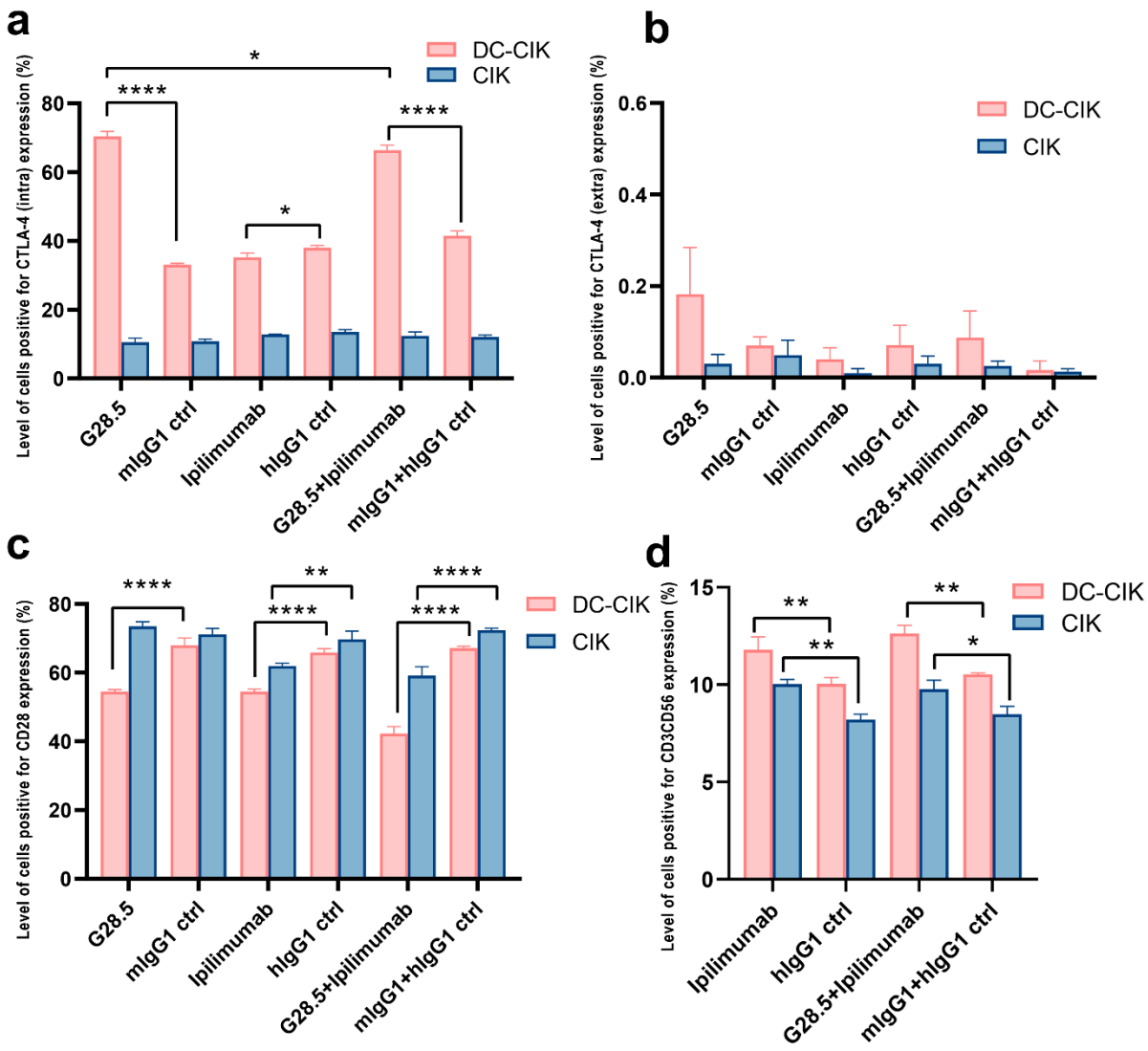

Fig. 3 G28.5 and ipilimumab have different effects on CTLA-4 expression of CIK cells. CIK cells treated with 10 μg/ml ipilimumab or hIgG1 control for nine days or without treatment were labeled by CellTrace™ Violet dye and cocultured with DCs at a ratio of 5:1. DC-CIK cells and CIK cells were treated with 10 μg/ml G28.5 or mIgG1 for another 48 h. The expression of intracellular and extracellular markers was detected by flow cytometry. Each bar represents mean ± SD of one representative donor. **a** G28.5 increased the intracellular CTLA-4 expression of CIK cells significantly via DCs compared to the isotype control, whereas ipilimumab showed an opposite effect. **b** G28.5 significantly increased the extracellular CTLA-4 expression of CIK cells via DCs. Ipilimumab slightly decreased the intracellular CTLA-4 expression, but there was no significance. **c** G28.5 inhibited CD28 expression of CIK cells via DCs, while ipilimumab directly inhibited that of CIK cells. **d** Ipilimumab increased the CD3+CD56+ population in DC-CIK and CIK cells. Intra: intracellular; extra: extracellular. (* $P < 0.05$, ** $P < 0.01$, **** $P < 0.0001$)

3.1.2.4 Assessing the direct effect of anti-CD40, anti-CTLA-4 and DC-CIK cells on RCC cell lines

We first performed CCK-8 assay to exclude any direct effect of G28.5 and ipilimumab on RCC cell lines (ACHN and Caki-2 cells). The CCK-8 results showed no apparent toxicity in ACHN cells after incubation with G28.5, ipilimumab, or the combination compared to isotype controls (Fig. 4a). The same result was observed on Caki-2 cells (Fig. 4b). Moreover, we tested the cytotoxicity of DC-CIK cells on RCC cells using flow cytometry (Fig. 4c). To mention, ACHN and Caki-2 cells were first labeled with CellTrace™ Violet dye so that they could be distinguished from DC-CIK cells. Tumor cells were then cocultured with DC-CIK cells at varying E/T ratios (1:1, 5:1, 10:1, 20:1, 40:1). We found that at E/T ratios above 5:1, DC-CIK cells efficiently killed ACHN and Caki-2 cells with the cytotoxicity ranging from 20% to 90%.

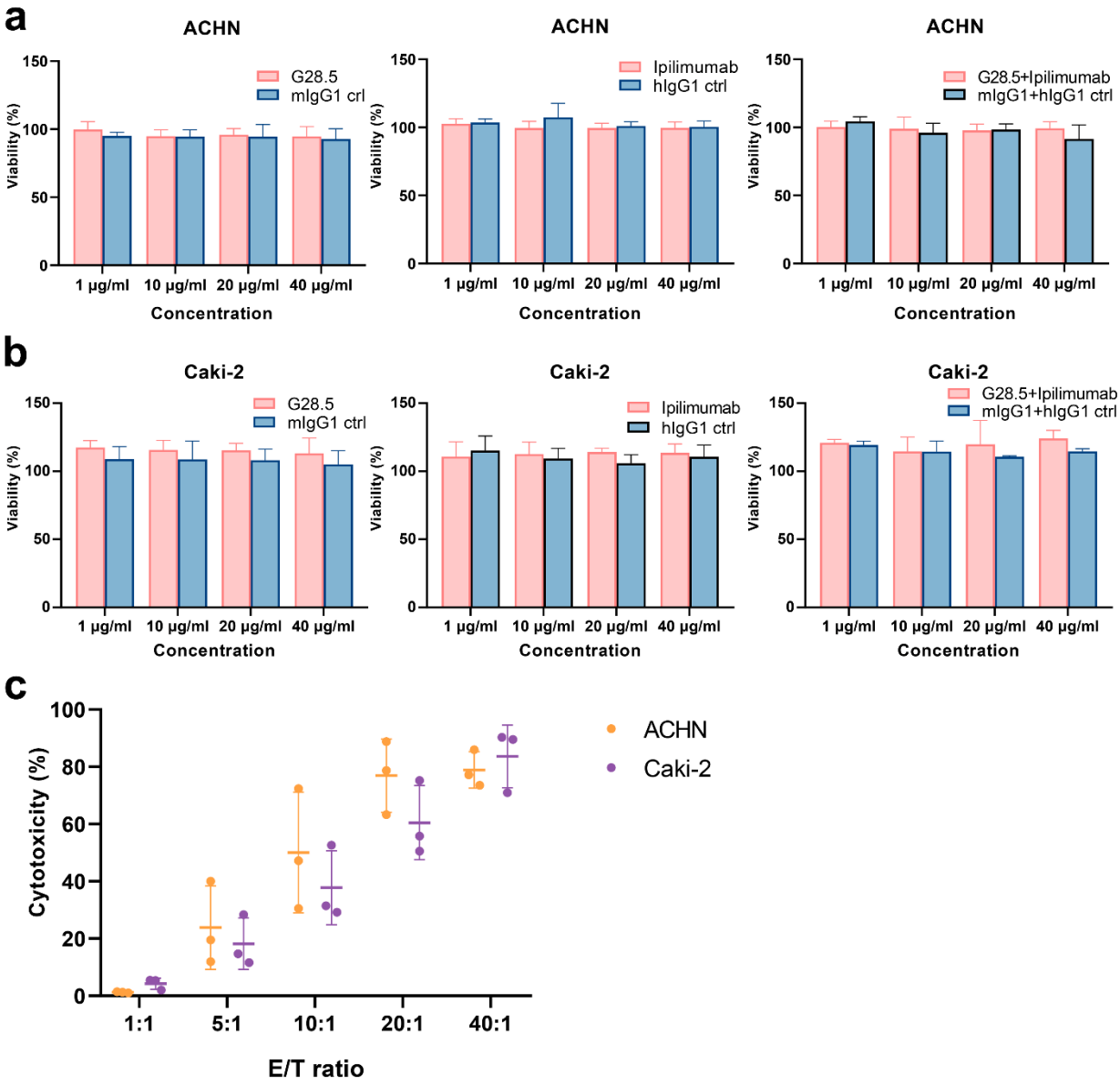

Fig. 4 Assessing the direct effect of anti-CD40, anti-CTLA-4 and DC-CIK cells on RCC cell lines. **a** No direct effect was observed from G28.5 and ipilimumab treatment against ACHN. ACHN cells were distributed in 96-well plates at 1 × 10^4 cells/well. G28.5 (left), ipilimumab (middle), the combination (right) and their isotype controls were added at different concentrations (1μg/ml, 10μg/ml, 20μg/ml, and 40μg/ml) for 24 h. Data are expressed as mean ± SD of one representative experiment. **b** No direct effect was observed from G28.5 and ipilimumab treatment against Caki-2. Caki-2 cells were distributed in 96-well plates at 0.5 × 10^4 cells/well and treated as **a**. **c** DC-CIK cells are cytotoxic against ACHN and Caki-2. ACHN (yellow) and Caki-2 (purple) cells were labeled by CellTrace™ Violet dye to distinguish them from DC-CIK cells. Tumor cells were distributed in 96-well plates and incubated 24 hours with DC-CIK cells at the E/T ratio of 1:1, 5:1, 10:1, 20:1, and 40:1. Then all cells were collected, and 7-AAD was added to detect dead cells by flow cytometry. Each bar represents mean ± SD of 3 donors.

3.1.2.5 Anti-CD40 antibody predominated over anti-CTLA-4 antibody for cytotoxicity, apoptotic effect and IFN-γ secretion of DC-CIK cells

As it has been assumed above that G28.5 combined with ipilimumab could promote the antitumor response of DC-CIK cells, we cocultured DC-CIK cells with tumor cells to see the effect of anti-CD40 and anti-CTLA-4 on them. We found that G28.5 significantly promoted the cytotoxicity of DC-CIK cells on ACHN by 13.2 ± 1.8% ($P < 0.0001$) in the G28.5 group and 17.3 ± 1.8% ($P < 0.0001$) in the combination group (Fig. 5a and b). Similar results were observed in the case of Caki-2, where G28.5 increased the cytotoxicity of DC-CIK cells by 8.7 ± 1.9% ($P = 0.007$), and the combination by 7.7 ± 1.9% ($P = 0.021$) (Fig. 5c and d). In contrast, the anti-CTLA-4 antibody ipilimumab did not increase the antitumor activity of DC-CIK cells on any cell lines.

We also investigated whether the apoptosis of RCC cells can be affected by DC-CIK cells with G28.5 and ipilimumab treatment. To mention, we detected both early and late apoptosis using Annexin V-FITC/7-AAD. In G28.5 group, early apoptosis of ACHN was significantly increased by 12.0 ± 1.9% ($P = 0.0004$) and by 13.1 ± 1.9% ($P = 0.0001$) when combined with ipilimumab (Fig. 6a and b). The enhanced effect on late apoptosis was also observed from G28.5 treatment (by 11.2 ± 0.9%, $P < 0.0001$) and from the combination (by 8.7 ± 0.9%, $P < 0.0001$). Similar to ACHN cells, the early apoptosis of Caki-2 was significantly increased in both G28.5 group (by 21.3 ± 1.8%, $P < 0.0001$) and the combination group (by 19.6 ± 1.8%, $P < 0.0001$) (Fig. 6c and d). Here again, anti-CTLA-4 antibody ipilimumab did not show any increase in the early or late apoptosis in any cell lines.

Next, we detected whether these two antibodies could promote the secretion of IFN-γ, a cytokine required for tumor killing by NK and cytotoxic T cells. The ELISA results showed that G28.5 alone or combined with ipilimumab significantly increased the IFN-γ secretion from DC-CIK cells against ACHN (by 228.6 ± 17.06 pg/ml, $P < 0.0001$ and 139.1 pg/ml ± 17.06, $P < 0.0001$, respectively) (Fig. 7a). Similar results were also found in case of Caki-2 cells (by 70.3 ± 7.4 pg/ml, $P < 0.0001$ and 90.1 ± 7.4 pg/ml, $P < 0.0001$, respectively). However, the anti-CTLA-4 antibody ipilimumab showed no obvious effect on the IFN-γ level in both cell lines. Considering the peculiar function of DC-CIK cells compared to CIK cells, we supplemented G28.5 in CIK cells (instead of

DC-CIK cells) and failed to detect any apparent increase (Fig. 7b). The result suggested that G28.5 could enhance the antitumor response of CIK cells solely by promoting the maturation and activation of DCs.

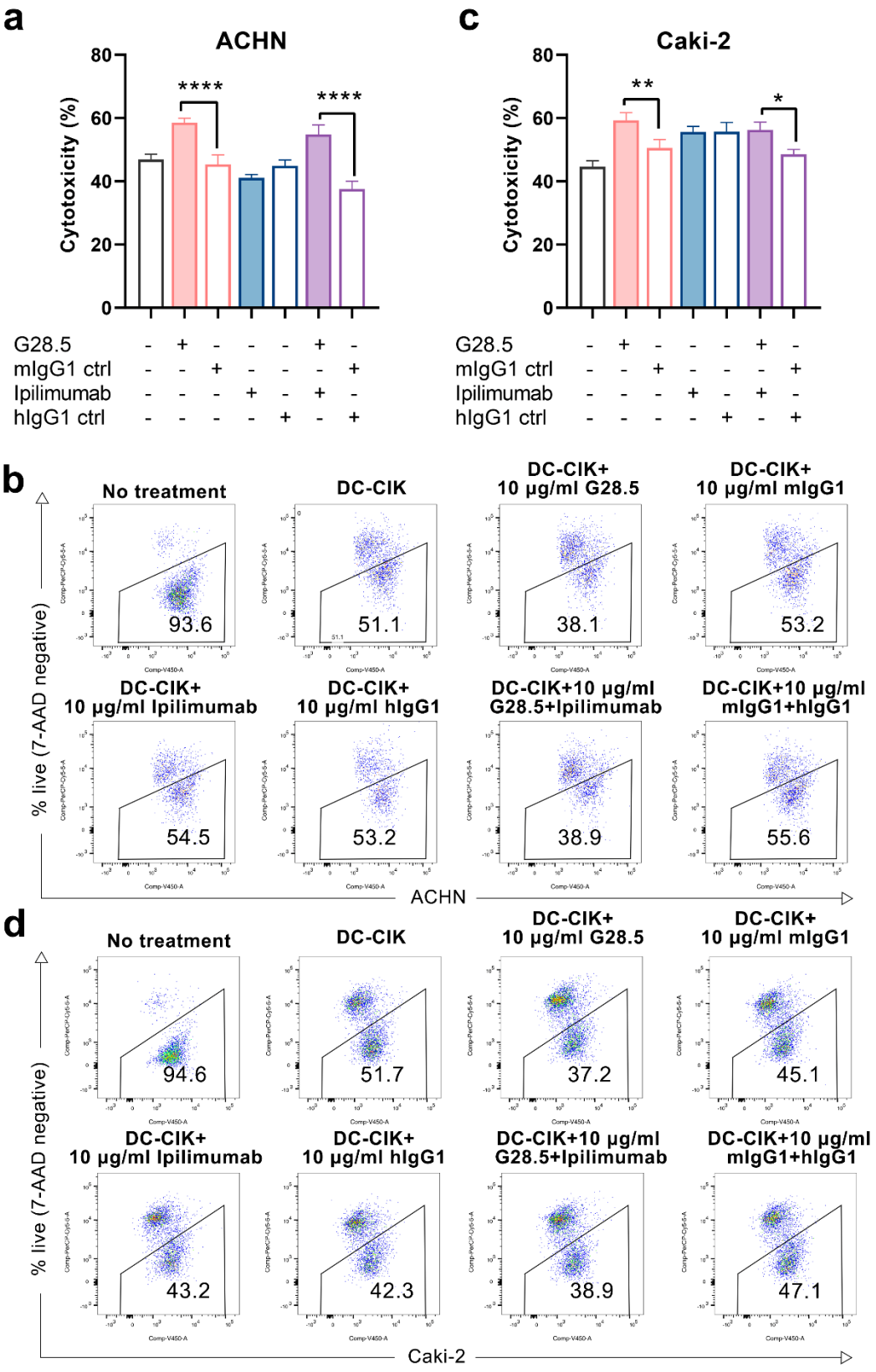

Fig. 5 Cytotoxicity of DC-CIK cells treated with G28.5 and ipilimumab against RCC cell lines. **a** Cytotoxicity of DC-CIK cells treated with G28.5 or ipilimumab against ACHN. ACHN cells were labeled by CellTrace™ Violet dye and distributed in 96-well plates at 3

× 10^4 cells/well. DC-CIK cells, ipilimumab or hIgG1 treated DC-CIK cells were then cocultured with ACHN cells at an E/T ratio of 10:1. After incubation with 10 μg/ml G28.5 or mIgG1 control for 24 h, all cells were collected, and 7-AAD was added to detect the dead cells by flow cytometry. Each bar represents mean ± SD of one representative donor. One representative flow cytometry analysis is shown in **b**. **c** Cytotoxicity of DC-CIK cells treated with G28.5 or ipilimumab against Caki-2 cells. Caki-2 cells were labeled by CellTrace™ Violet dye and distributed in 96-well plates at 1.2 × 10^4 cells/well. The following procedures were performed as above. One representative flow cytometry analysis is shown in **d**. (* $P < 0.05$, ** $P < 0.01$, **** $P < 0.0001$)

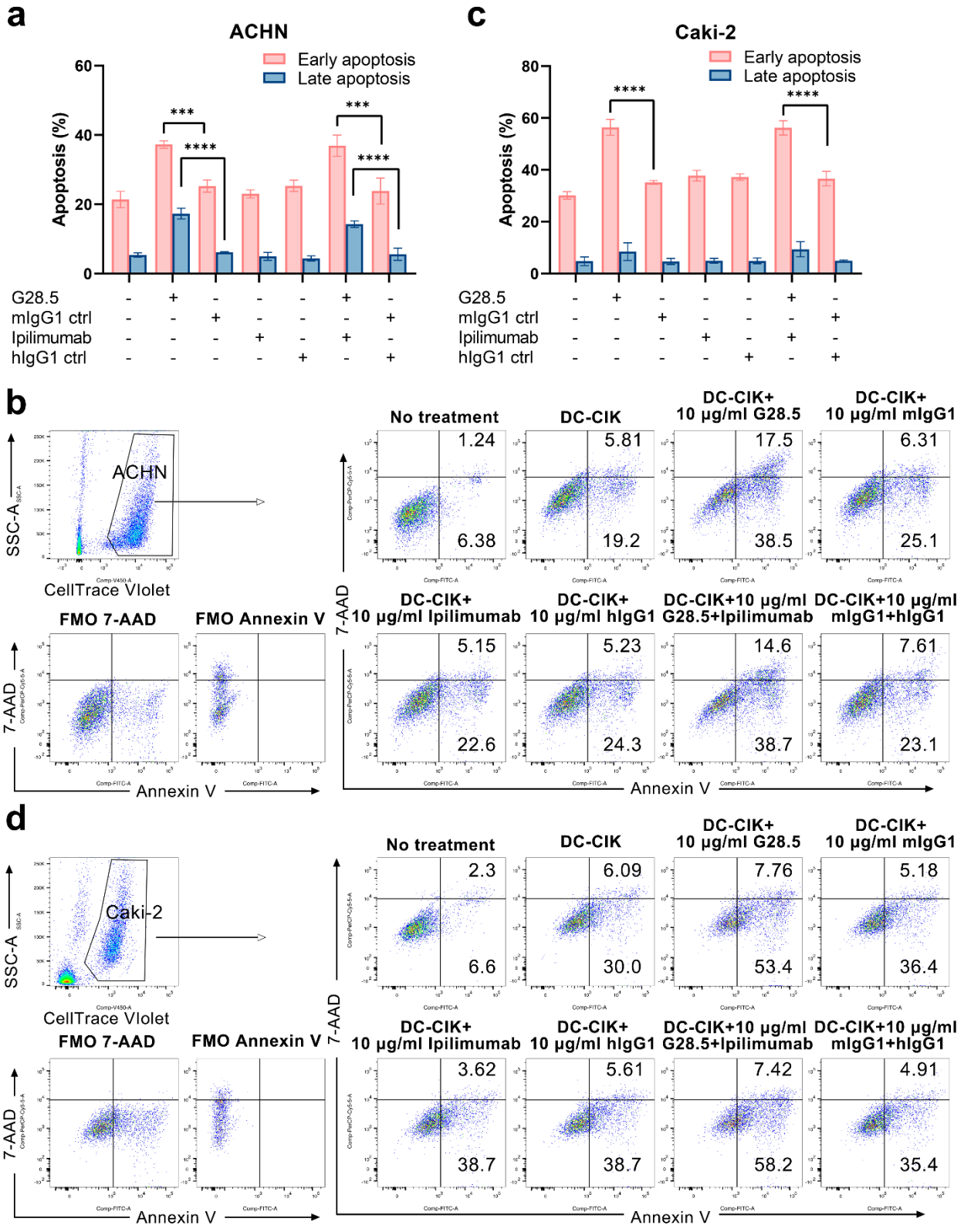

Fig. 6 Apoptosis of RCC cells treated with DC-CIK cells combined with G28.5 and ipilimumab. **a** Early and late apoptosis of ACHN cells treated with DC-CIK cells in combination with G28.5 and ipilimumab. ACHN cells were labeled by CellTrace™ Violet dye and distributed in 96-well plates at 3 × 10^4 cells/well. Tumor cells were cocultured

with DC-CIK cells, ipilimumab or hIgG1 treated DC-CIK cells at an E/T ratio of 5:1. After incubation with 10 μg/ml G28.5 or mIgG1 control for 10-14 h, Annexin V-FITC/7-AAD was used to detect the early (Annexin V+7-AAD-) and late apoptosis (Annexin V+7-AAD+) by flow cytometry. Each bar represents mean ± SD of one representative donor. One representative flow cytometry analysis is shown in **b**. **c** Early and late apoptosis of Caki-2 cells treated with DC-CIK cells in combination with G28.5 and ipilimumab. Caki-2 cells were labeled by CellTrace™ Violet dye and distributed in 96-well plates at 1.2×10^4 cells/well. The following procedures were performed as **a**. One representative flow cytometry analysis is shown in **d**. (*** $P < 0.001$, **** $P < 0.0001$)

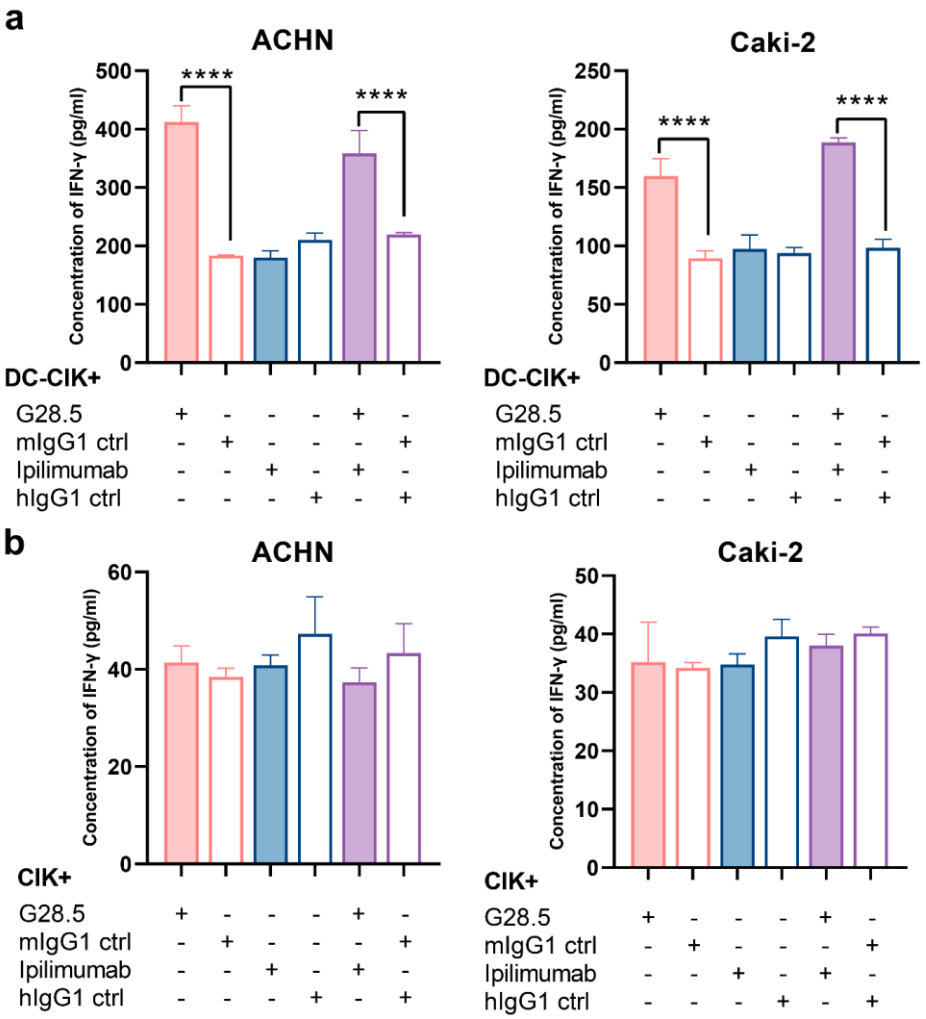

Fig. 7 Effect of G28.5 and ipilimumab on IFN-γ secretion of DC-CIK and CIK cells. **a** The IFN-γ secretion of DC-CIK cells against ACHN (left) and Caki-2 (right) cells. DC-CIK cells, ipilimumab or hIgG1 treated DC-CIK cells were cocultured with tumor cells (5×10^4 cells/well) at a ratio of 10:1. Cells were incubated with 10 μg/ml G28.5 or mIgG1 control for 24 h. At the end of incubation, the supernatant was collected to determine the concentration of IFN-γ by ELISA. Each bar represents mean ± SD of one representative donor. **b** The IFN-γ secretion of CIK cells against ACHN (left) and Caki-2 (right) cells. (**** $P < 0.0001$)

3.1.2.6 Ipilimumab did not alter the Treg population in CIK cells

Since it was not observed that ipilimumab enhanced the antitumor response of DC-CIK cells, we sought to investigate whether another independent determinant (e.g., Tregs) may be a contributing factor. It has been discussed that tumor regression caused by anti-CTLA-4 antibodies may rely on a selective reduction of Tregs but not checkpoint blockade (Du et al., 2018; Selby et al., 2013). Therefore, we compared the Treg population in CIK cells before and after ipilimumab treatment, as described previously (Yano et al., 2014). Similar to the results of Yano *et al*., after 14 days' incubation of activated T cells with 10 μg/ml ipilimumab, Tregs (CD3+CD4+CD25+CD127low) were significantly reduced by 4.2 ± 2.3% ($P = 0.034$) in activated T cells compared to the control group (Fig. 8a and d). Besides, a decrease in the CD4/CD8 ratio was also observed ($P = 0.326$) (Fig. 8b and c). However, when CIK cells were incubated with 10 μg/ml ipilimumab, the proportion of Tregs remained unaffected ($P = 0.567$) (Fig. 9a and b). The results may partially explain why the addition of ipilimumab did not enhance the antitumor response of DC-CIK cells. The hypothesized mechanism of anti-CD40 and anti-CTLA-4 antibodies on DC-CIK cells is shown in Fig. 9c.

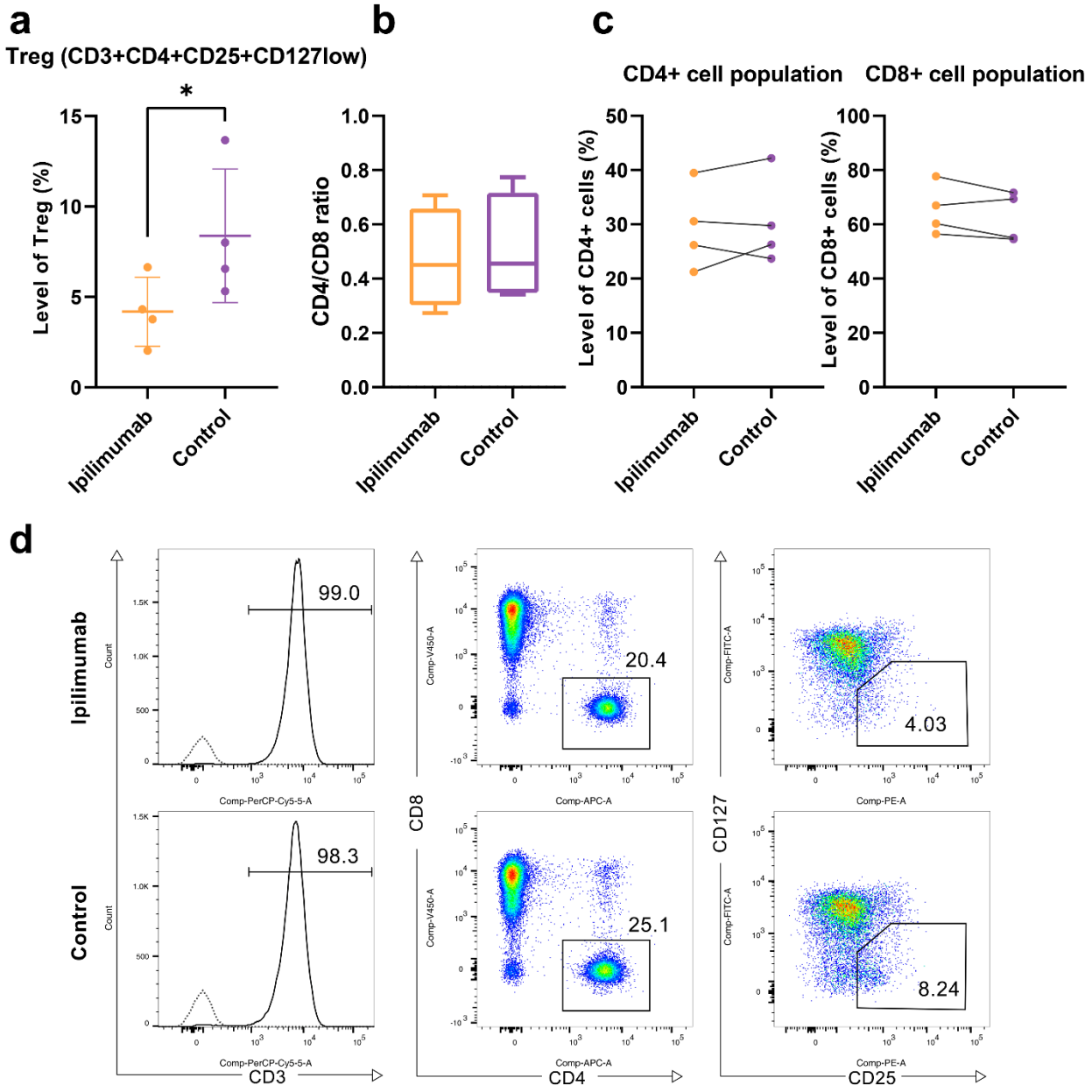

Fig. 8 Ipilimumab decreases the Treg population in activated T cells. **a** Treg population in activated T cells after treatment with ipilimumab or isotype control. T cells in peripheral blood mononuclear cells were activated by 20 ng/mL of anti-CD3 monoclonal antibody and expanded with 100 IU/mL of IL-2 according to the protocol of Yano *et al*. (Yano et al., 2014). Activated T cells were incubated with the presence or absence of 10 μg/ml ipilimumab for 14 days. Tregs (CD3+CD4+CD25+CD127low) in activated T cells were detected by flow cytometry. Each bar represents the mean ± SD of four donors. (* $P < 0.05$) **b** A slightly decreased CD4/CD8 ratio is shown in activated T cells treated with ipilimumab. **c** The proportion of CD4+ (left) and CD8+ (right) cells were detected in the ipilimumab and control groups. **d** One representative flow cytometry analysis is shown.

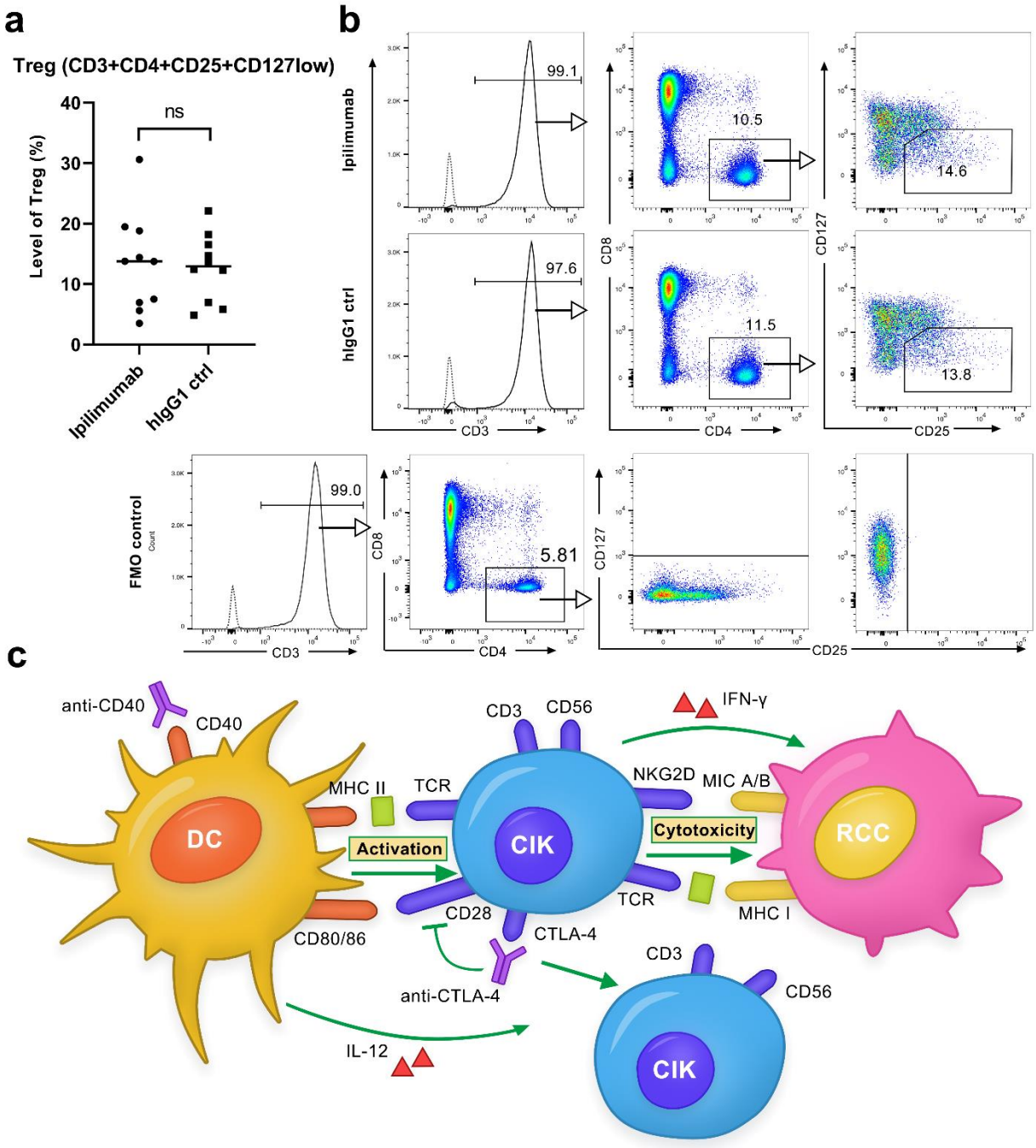

Fig. 9 Ipilimumab is ineffective in decreasing the Treg population in CIK cells. **a** Treg population in CIK cells after treatment with ipilimumab or isotype control. 10 μg/ml ipilimumab or hIgG1 control was added to CIK cells only once at the initiation of culture. Tregs (CD3+CD4+CD25+CD127low) in CIK cells of ten donors were detected by flow cytometry. Each bar represents the mean ± SD of ten donors. (*ns* not significant) **b** One representative flow cytometry analysis is shown. **c** Schematic of the effect of anti-CD40 and anti-CTLA-4 antibodies on DC-CIK cells. Anti-CD40 antibody-activated DCs increased the cytotoxicity of CIK cells against RCC cells, whereas the anti-CTLA-4 antibody had a very restrictive effect on the antitumor response. The anti-CTLA-4 antibody increased the proportion of CD3+CD56+ effector cells but decreased CD28

expression.

3.1.3 Discussion

Clinical studies based on CIK cells have shown big promise in the treatment of patients with cancer, including RCC (Zhang et al., 2020). CIK cells have also been licensed in various countries, including Germany. But considering the patients who are non-responsive or refractory to the treatment, several efforts are still being performed to make it more efficient. One convenient option that is worth considering is to promote the antitumor response of CIK/DC-CIK cells. Recent studies also provided insights into the enhancement of their cytotoxicity (Wu et al., 2021; Yu et al., 2019). In the current manuscript, we sought to investigate whether the combination of anti-CD40 and anti-CTLA-4 antibodies can considerably enhance the antitumor response of DC-CIK cells against RCC cell lines. To achieve this, we first characterize the phenotype of CIK cells and DCs, and observed that the anti-CD40 antibody (G28.5) increased the CD3+CD56+ population of CIK cells via DCs. In addition, we found that the antitumor response of DC-CIK cells was significantly improved by G28.5, while the CTLA-4 inhibitor ipilimumab showed a very restrictive effect.

It has been known that tumor cell escape often occurs through impaired antigen recognition by the immune system or the establishment of an immunosuppressive state in tumor microenvironment (e.g., Tregs) (Schreiber et al., 2011). We therefore sought to enhance the tumor-killing activity of DC-CIK cells in two distinct ways: First, by promoting maturation and activation of antigen-presenting DCs through CD40 ligation, and second, by suppressing inhibitory signaling in the effector cells or reducing Tregs by CTLA-4 blockade. In this context, it has been previously discussed that the combination of anti-CD40 and anti-CTLA-4 antibodies accompanying a liposomal peptide or adenoviral vaccine considerably enhanced the CTL responses against tumor cells (Ito et al., 2000; Sorensen et al., 2010). And CD40 activation on DC cells has previously been demonstrated to increase Th1 cell proliferation (Fallarino et al., 2002). In our analysis, we first found the possibility that G28.5 in combination with ipilimumab might increase the antitumor efficacy of DC-CIK cells compared to G28.5 or ipilimumab alone, primarily by reducing inhibitory CTLA-4 signaling and proliferating CD3+CD56+ effector cells. However, our results showed that anti-CD40 antibody predominated over anti-CTLA-4

antibody for cytotoxicity, apoptotic effect and IFN-γ secretion of DC-CIK cells against RCC cells. To mention, despite some clinical differences in the RCC cell lines (Caki-2: male/69 years, clear cell renal cell carcinoma; ACHN: male/22 years, renal cell adenocarcinoma), our results were consistent in both of them. Therefore, the possibility of heterogeneity between these cancer cell lines (in addition to genetic-epigenetic variations) as a confounding factor can be excluded, as discussed by Sharma *et al*. (Sharma et al., 2020).

To determine the potential reason for ipilimumab inefficacy, we further investigated whether another independent factor (e.g., Tregs) might play a role. For instance, it has been discussed that tumor regression caused by anti-CTLA-4 antibodies may rely on a selective reduction of Tregs (Du et al., 2018; Selby et al., 2013). Therefore, we compared the population of Tregs in CIK cells before and after ipilimumab treatment, but no obvious changes were observed. However, we noticed that both G28.5 and ipilimumab significantly reduced the expression of CD28 in CIK cells. It is well known that CD28 has a similar structure to CTLA-4 but has an opposite effect on T cell immunity. CD28-mediated co-signaling is related to cytokine production and T cell proliferation (Rudd et al., 2009). In context to our data, how this decrease in CD28 accounts for the crosstalk between ipilimumab and CIK cells needs further investigation. Notably, the expression of CTLA-4 decreased sharply after two weeks of culture, suggesting that the inhibitory signaling of CTLA-4 may not play an essential role in the cytotoxicity of CIK cells. It is worth mentioning that, a) whether these observed changes are RCC specific or also occur in other cancers needs to be further investigated; b) translating our results to in vivo models will also provide more information about the contribution of the tumor microenvironment.

3.2 Study 2: Integrative analysis of key candidate genes and signaling pathway in autoimmune thyroid dysfunction related to anti-CTLA-4 therapy by bioinformatics

3.2.1 Introduction

Cytotoxic T lymphocyte-associated antigen-4 (CTLA-4), a critical negative regulator of T cell responses, is the first immune checkpoint to be targeted clinically (Pardoll, 2012). As discussed in study 1, CTLA-4 blockade has provided an effective treatment option for various malignancies, including RCC. CTLA-4 is a type 1 transmembrane glycoprotein of the immunoglobin superfamily sharing 31% amino acid identity with CD28 (Brunet et al., 1987). CTLA-4 and CD28 share identical ligands, CD80 and CD86, but CTLA-4 has a much higher affinity for both ligands (Azuma et al., 1993; Freeman et al., 1993; Hathcock et al., 1993; Linsley et al., 1991; Linsley et al., 1994). Although the exact mechanism of CTLA-4 signaling is still under debate, it has been proposed that CTLA-4 inhibits T cell activity by competing with CD28 for CD80/CD86 engagement and delivering an inhibitory signal by its cytoplasmic tail (Egen and Allison, 2002; Riley et al., 2002; Schneider et al., 2002). Anti-CTLA-4 antibodies, such as ipilimumab and tremelimumab, can exert their antitumor effects via activating CD8+ effector T cells and modulating the function of CD4+ T cells (Pardoll, 2012). Ipilimumab alone or combined with nivolumab has demonstrated overall survival benefits in patients suffering from metastatic melanoma, metastatic RCC, and other malignancies (Hammers et al., 2015; Hodi et al., 2010).

Despite its favorable antitumor efficacy, the blockade of CTLA-4 also leads to immune-related adverse events (IRAEs). IRAEs are described as autoimmune manifestations that result from the induction of a tolerance break against the tumor and involve a wide range of organ systems (Barroso-Sousa et al., 2018). Autoimmune thyroid dysfunction is one of the common IRAEs reported clinically and at potentially high risk after checkpoint inhibitor treatment. Autoimmune thyroid dysfunction includes hypothyroidism and hyperthyroidism, especially after single CTLA-4, PD-1 blockade therapy, or the combination treatment regime (Byun et al., 2017; Morganstein et al., 2017). The autoimmune thyroid dysfunction is either caused by primary thyroid gland

disorders or as a result of pituitary dysfunction, both induced by immune checkpoint blockade (Postow, 2015). Clinical studies have shown that the incidence of primary and secondary hypothyroidism after administration of ipilimumab was 5.6% and 7.6% of the patients, respectively (Postow, 2015; Ryder et al., 2014). However, the time point of primary hypothyroidism occurrence was not clarified, which could range from 5 months to 3 years. Hyperthyroidism is usually found as a transient symptom at the beginning of autoimmune thyroiditis or associated with Graves' disease after anti-CTLA-4 treatment. Persistent primary hyperthyroidism is significantly less frequent than hypothyroidism, with an occurrence of 1.7% (Barroso-Sousa et al., 2018). The patients who develop autoimmune thyroiditis after CTLA-4 blockade therapy exhibit symptoms such as pain, hand tremor, periorbital swelling, or tachycardia (Min et al., 2011). These symptoms have a considerable negative influence on the quality of life of patients who are suffering from cancer. Therefore, it is critical to identify proper strategies to diagnose and treat autoimmune thyroid dysfunction after anti-CTLA-4 therapy effectively.

Microarrays have become a valuable method to analyze the gene expression pattern on a global basis (Townsend et al., 2003). Gene Expression Omnibus (GEO) database is a repository for high-throughput gene expression data and is accessible to the public (Edgar et al., 2002). Gene data stored in the platform makes it possible to identify differentially expressed genes (DEGs) and find promising biomarkers for human diseases (Kulasingam and Diamandis, 2008). Text mining is a powerful tool to extract large amounts of biological information from various written resources by computer (Gupta and Lehal, 2009). Here, A public tool pubmed2ensembl is used to perform text mining. Pubmed2ensembl is a database based on an extended version of the BioMart data mining system. It can find relevant literature on functionally related genes (Baran et al., 2011).

As the most commonly used mammalian research model, the laboratory mouse provides a valuable and accessible method for investigating and elucidating the genetic foundation of human diseases. The rapid development in comparative genetics makes the human and mouse homolog map more detailed. It increases our understanding of the high conservation of cellular and metabolic pathways between mice and humans on a molecular and genetic level (Darling and Abbott, 1992; Lin et al., 2014). Studies have shown that gene expression between the corresponding tissues from different

organisms is more similar and conserved than the alternative tissues from identical organisms (Merkin et al., 2012). Mouse gene chips not only provide a complete expression profile of the mouse genome but also give us an ideal reference to investigate the underlying mechanism of human diseases on a genetic level.

Herein, we downloaded GSE32445 and GSE58062, the mouse hypothyroidism and hyperthyroidism gene expression profiles, respectively, from the GEO database. R language was utilized to standardize and analyze the microarray datasets to obtain DEGs. We then converted the mouse DEGs to their human orthologous genes to deduce the expression pattern of human genes from their mouse orthologues. Text mining about anti-CTLA-4 therapy was then performed by the online tool pubmed2ensembl. After achieving the common genes from microarrays and text mining, the integrated DEGs were subsequently analyzed via GO enrichment and KEGG pathway. The protein-protein interaction (PPI) networks were constructed using the online Search Tool for the Retrieval of Interacting Genes (STRING) and Cytoscape software to identify the candidate hub genes and highly related functional modules.

3.2.2 Results

3.2.2.1 Identification of integrated DEGs related to hypothyroidism/ hyperthyroidism and anti-CTLA-4 therapy

As it is shown in Fig. 10, the hypothyroidism gene expression series GSE32445 and hyperthyroidism gene expression series GSE58062 were first normalized. After being screened by the limma package, a total of 1270 DEGs between hypothyroid samples and normal controls were identified from the GSE32445 dataset, including 558 upregulated genes and 712 downregulated genes. 475 DEGs between hyperthyroid samples and normal controls were defined from the GSE58062 dataset, including 293 upregulated genes and 182 downregulated genes. The overall distribution and top 100 DEGs of the two datasets are shown in volcano plots (Fig. 11a and c) and heatmaps (Fig. 11b and d), respectively.

The DEGs acquired from the two mouse microarray datasets were converted to their human orthologs. A total of 948 human DEGs were obtained in the hypothyroidism group, containing 420 upregulated genes and 528 downregulated genes (Table 1a). 341

DEGs related to hyperthyroidism were identified and consist of 216 upregulated genes and 125 downregulated genes (Table 1b).

The tool pubmed2ensembl was used to perform text mining, with “CTLA-4”, “ipilimumab,” and “tremelimumab” as the queries. 452 human genes associated with anti-CTLA-4 therapy were revealed by text mining (Table 2). We next compared the DEGs from microarray data to the gene list derived from text mining. Intersections of genes were obtained, involving 22 genes in the hypothyroidism group and 17 genes in the hyperthyroidism group (Fig. 12).

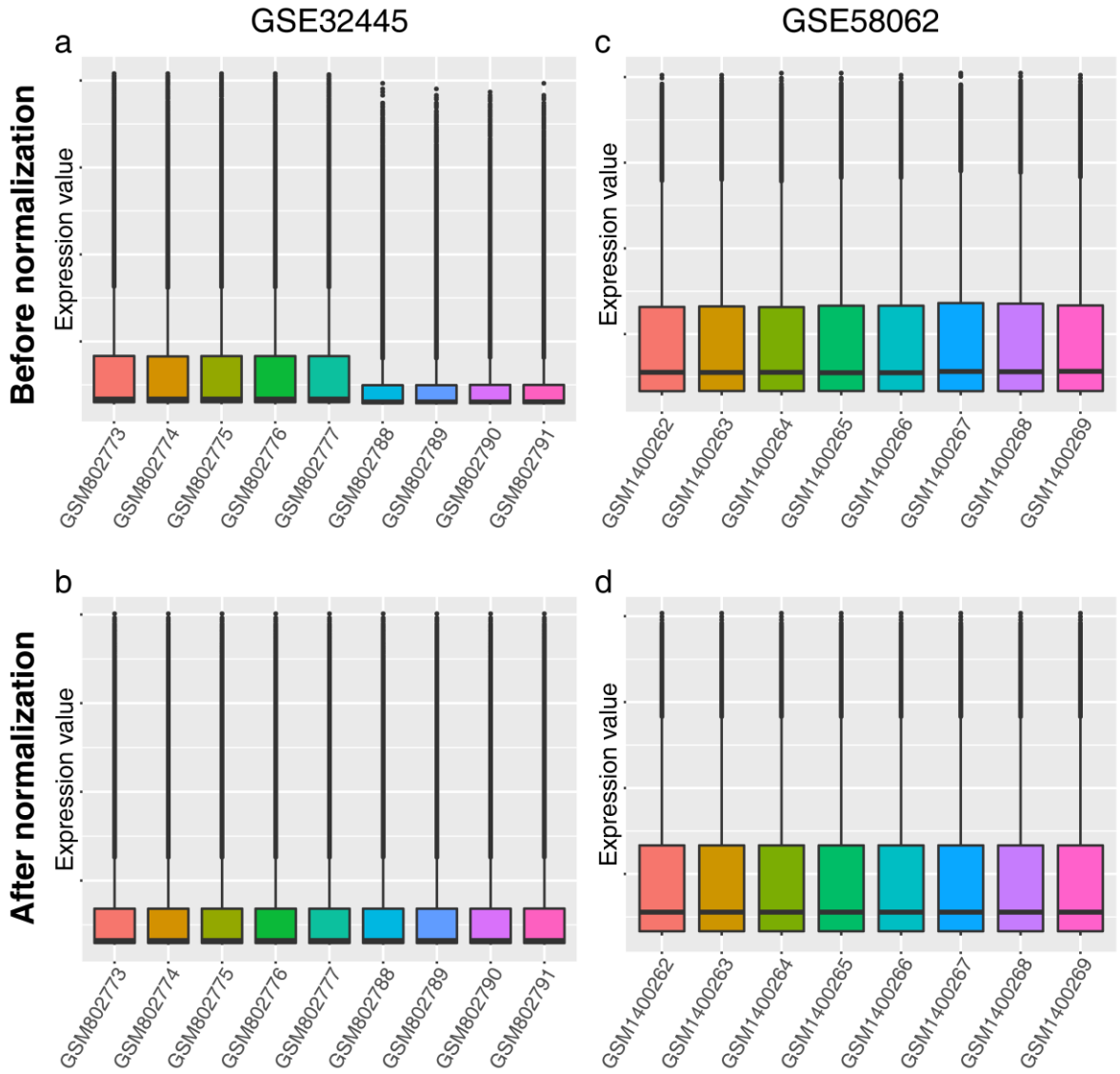

Fig. 10 Normalization of gene expression profile matrix. **a, b** Before and after normalization of the hypothyroidism GSE32445 dataset. **c, d** Before and after normalization of the hyperthyroidism GSE58062 dataset.

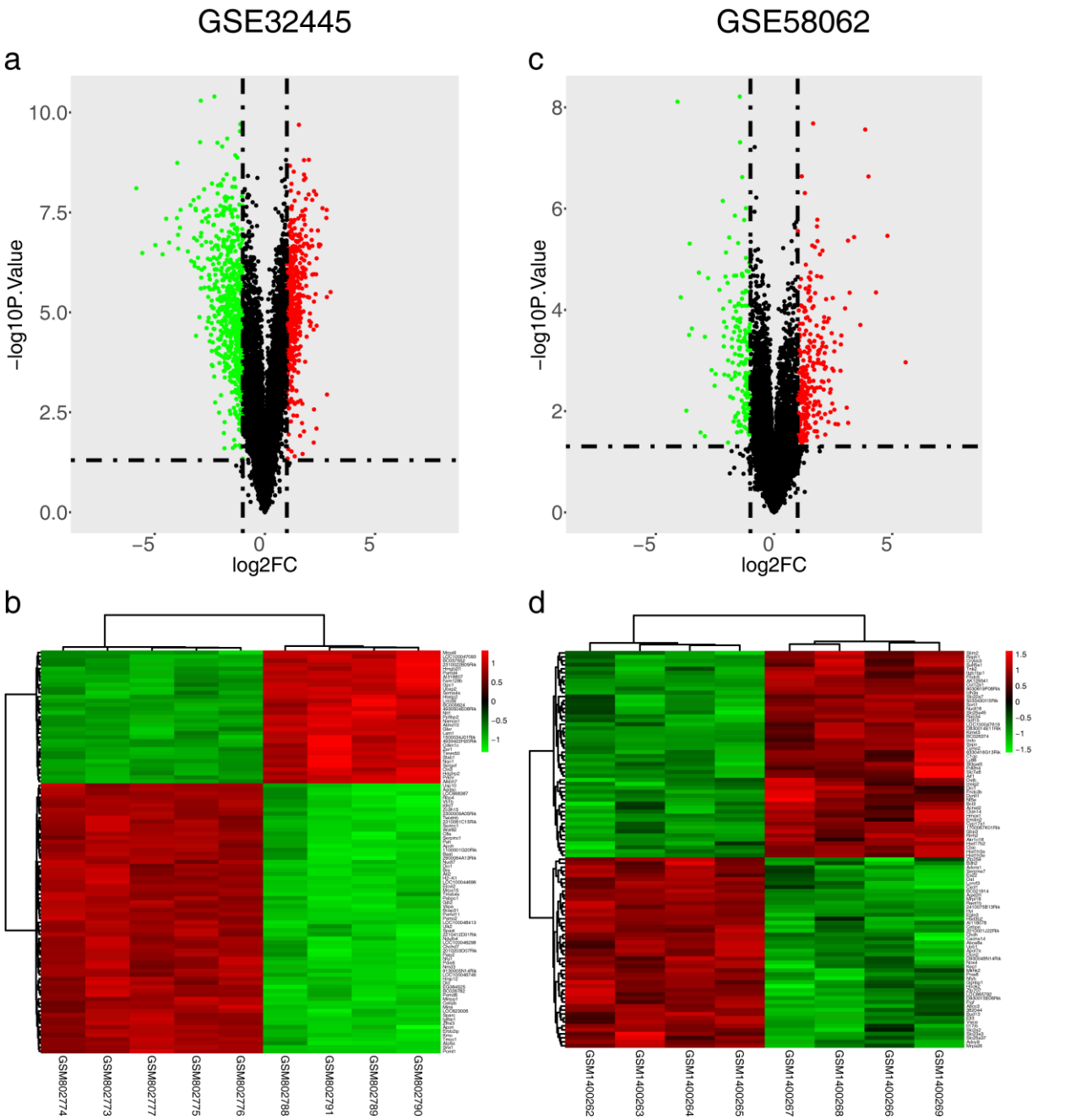

Fig. 11 Differentially expressed genes between hypothyroid/hyperthyroid and control groups. **a, b** Volcano plot and cluster heat map of the top 100 differentially expressed genes from GSE32445. **c, d** Volcano plot and cluster heat map of the top 100 differentially expressed genes from GSE58062. Red represents the upregulated genes based on |log2FC| > 1 and P value < 0.05, and green represents the downregulated genes based on the same statistical requirements.

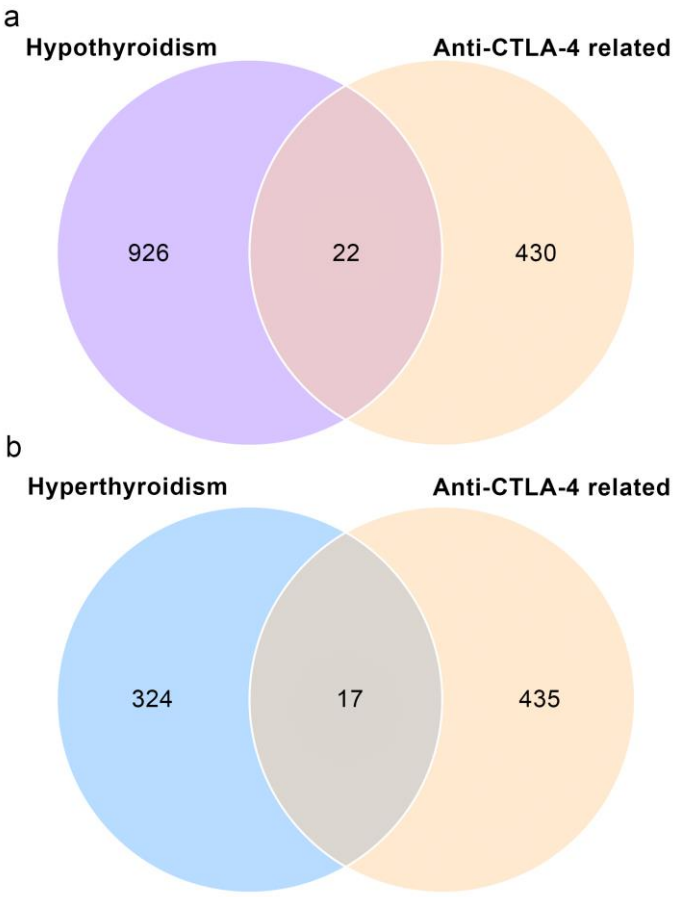

Fig. 12 Venn diagram of DEGs from microarray data and genes list from text mining. **a** Intersection of genes between DEGs generated from GSE32445 and anti-CTLA-4 gene list from text mining. **b** Intersection of genes between DEGs generated from GSE58062 and anti-CTLA-4 gene list from text mining. DEGs, differentially expressed genes.

3.2.2.2 Functional enrichment analysis

GO and KEGG enrichment analysis was performed by the Database for Annotation Visualization and Integrated Discovery (DAVID) based on the integrated DEGs achieved above. The enrichment analysis was done to investigate the correlated biological function of the integrated DEGs of autoimmune thyroid dysfunction related to anti-CTLA-4 therapy. In the results of GO analysis, 10 biological process (BP) terms, 10 cell component (CC) terms, and 4 molecular function (MF) terms were identified in the integrated DEGs of hypothyroidism with a P value < 0.05 as the significant threshold (Fig. 13). 5 genes were enriched in the BP term “negative regulation of apoptotic process,” 12 genes fell into in the CC term “extracellular exosome,” and 7 genes were involved in the MF term “identical protein binding” (Table 3a). In hyperthyroidism,

integrated DEGs were significantly enriched in 21 GO terms, including 8 BP terms, 6 CC terms, and 7 MF terms (Fig. 14). The genes were primarily enriched in the following terms: “regulation of immune response” in BP, “extracellular exosome” in CC, and “drug binding” in MF (Table 3b). These are the top 3 terms of GO annotation, with the integrated genes enriched most significantly.

The KEGG enrichment analysis revealed that the integrated DEGs were significantly enriched in the KEGG pathway “tuberculosis” in the hypothyroidism group and “osteoclast differentiation,” “tuberculosis” in the hyperthyroidism group (Fig. 15). Notably, even though the other three pathways “thyroid cancer”, “focal adhesion” and “prion diseases” in hypothyroidism were not considered significant, the gene MAPK1 was enriched in all the hypothyroidism related KEGG pathways (Table 4).

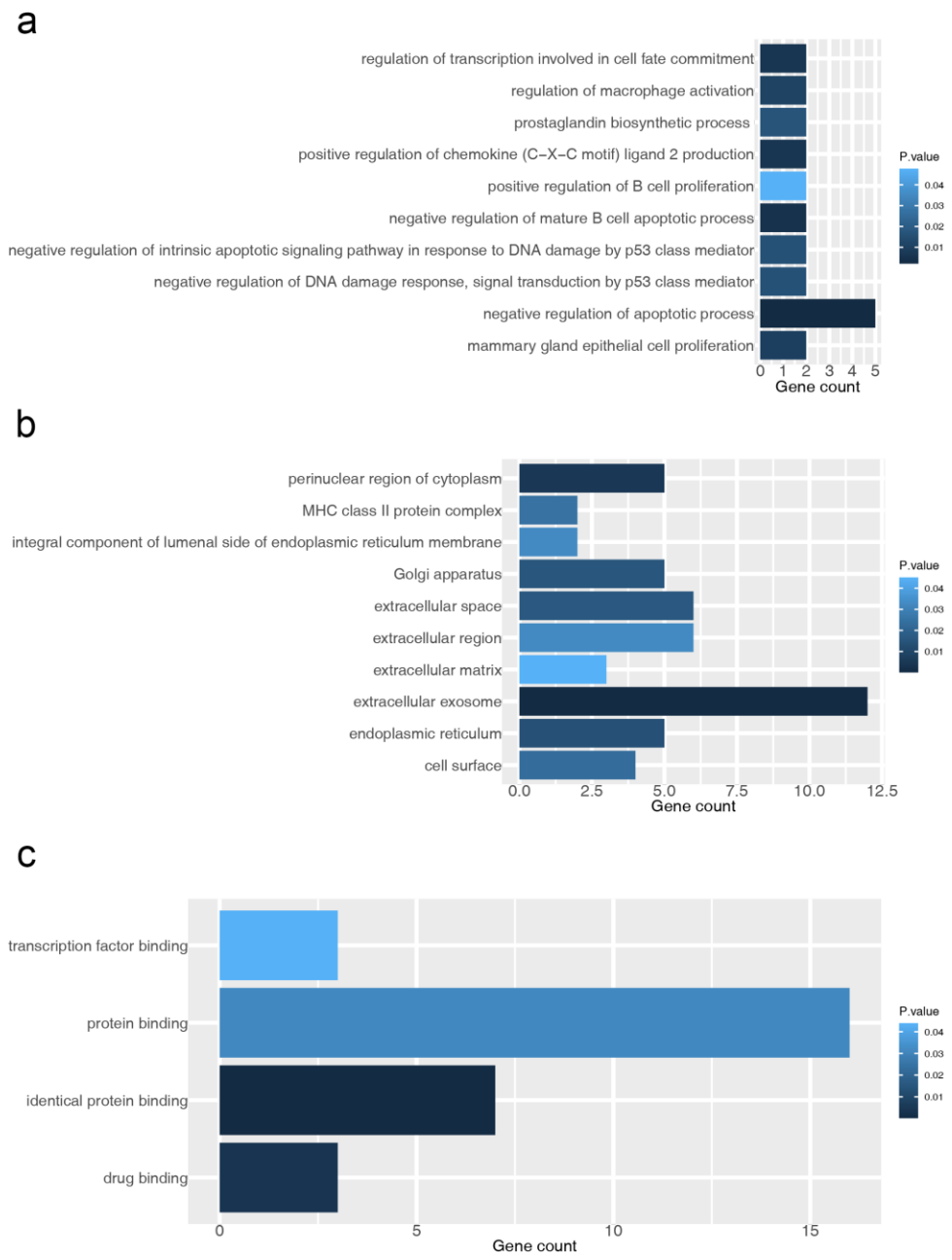

Fig. 13 GO analysis of the common genes associated with hypothyroidism and anti-CTLA-4 therapy. **a** biological process. **b** cell component. **c** molecular function.

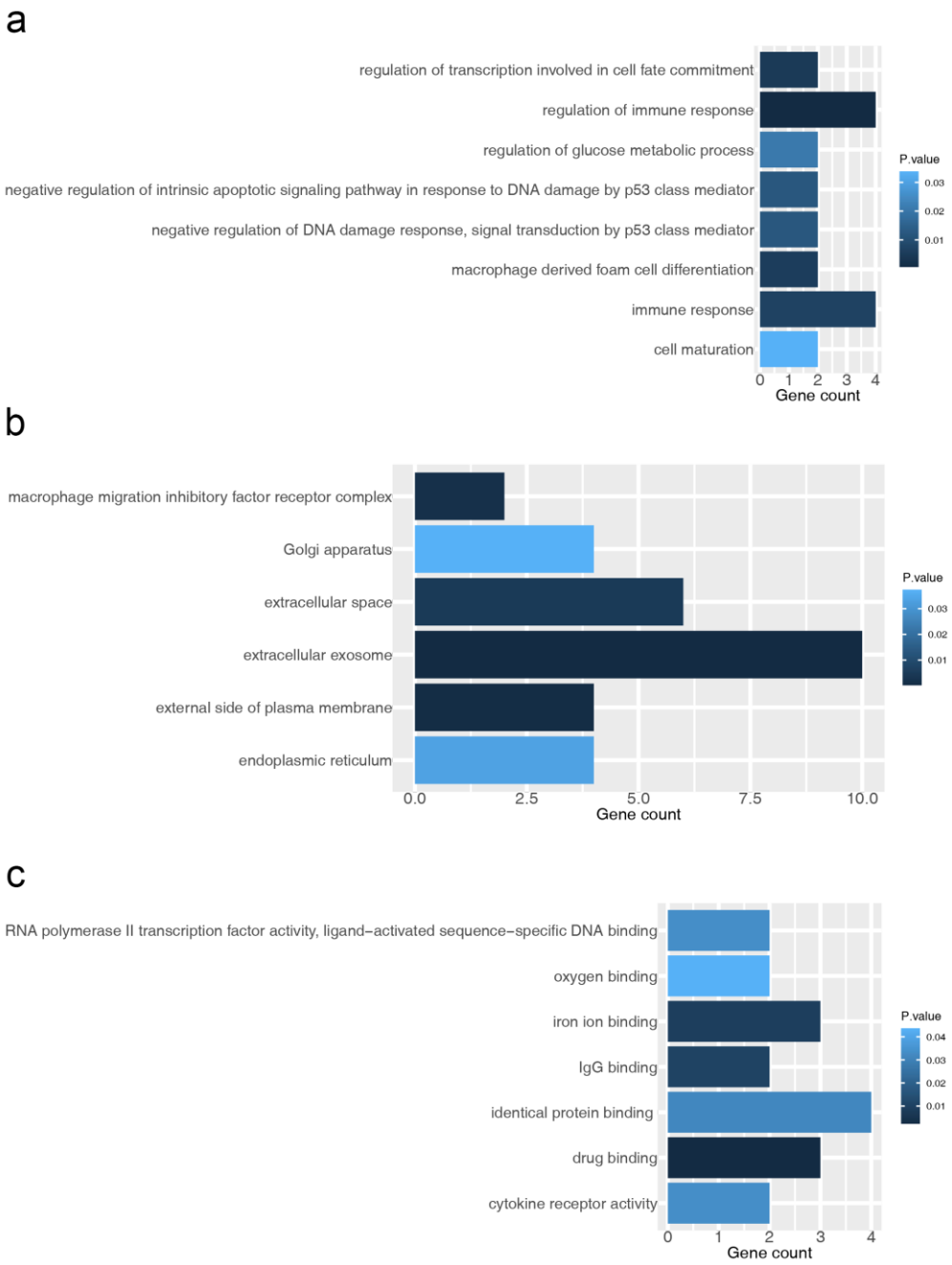

Fig. 14 GO analysis of the common genes associated with hyperthyroidism and anti-CTLA-4 therapy. **a** biological process. **b** cell component. **c** molecular function.

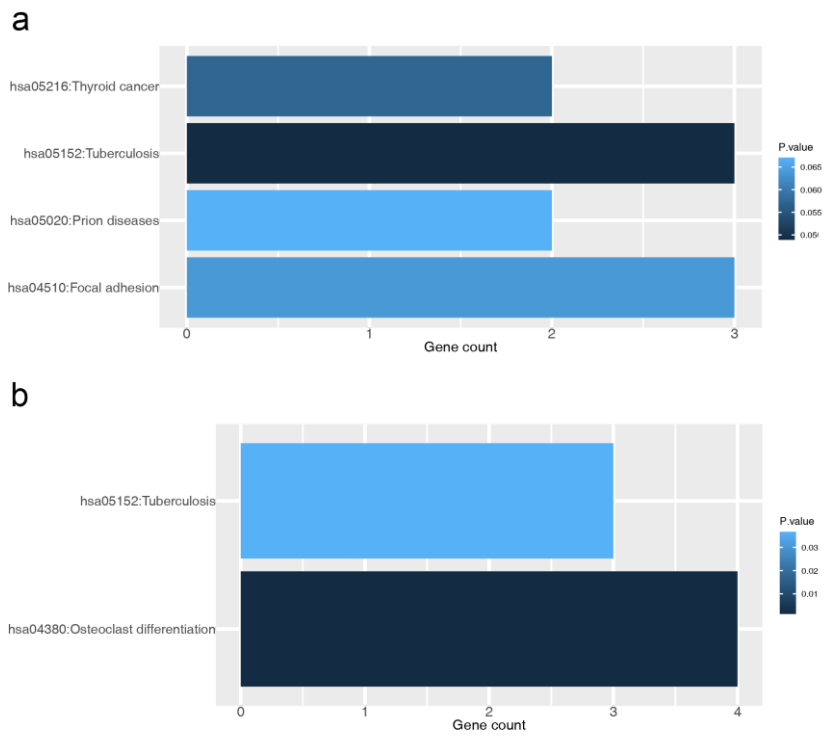

Fig. 15 KEGG pathway enrichment of the integrated DEGs associated with autoimmune thyroid dysfunction and anti-CTLA-4 therapy. **a** hypothyroidism. **b** hyperthyroidism. DEGs, differentially expressed genes

3.2.2.3 Construction and module analysis of PPI network

PPI network, module analysis, and visualization were performed by the STRING database and Cytoscape platform. The protein interaction was generated based on the 22 integrated DEGs in the hypothyroidism group and 17 DEGs in the hyperthyroidism group. In hypothyroidism, a PPI network containing 23 interactions was constructed (Fig. 16a), whereas the PPI network in hyperthyroid group was generated with 24 interactions (Fig. 16b). According to the degree value, the top five hub genes extracted from the hypothyroidism group were ALB (albumin), MARK1 (microtubule affinity regulating kinase 1), SPP1 (secreted phosphoprotein 1), PPARG (peroxisome-proliferator activated receptor gamma) and MIF (macrophage migration inhibitory factor). On the other hand, in the hyperthyroid group, the top five hub genes were ALB, FCGR2B (Fc fragment of IgG receptor IIb), CD44, LCN2 (lipocalin 2), and CD47 (Table 5).

MCODE algorithm was performed to detect highly interconnected subnets that are usually protein complexes and parts of pathways based on the topological structure. One highly connected cluster was constructed with 5 nodes and 9 edges from the PPI

network of hypothyroidism, including 3 upregulated and 2 downregulated genes (Fig. 16c). A cluster from the network of hyperthyroidism was generated with 4 nodes and 6 edges, containing 2 upregulated and 2 downregulated genes (Fig. 16d). Further functional enrichment analysis of the identified modules revealed that genes in the module of hypothyroidism were primarily enriched in the GO terms of “response to stress,” “perinuclear region of cytoplasm”, “identical protein binding” and KEGG pathway of “PI3K-Akt signaling pathway” (Table 6a). Genes in the module of hyperthyroidism mainly fell into the GO terms of “response to nutrient,” “Golgi apparatus” and “drug binding” (Table 6b).

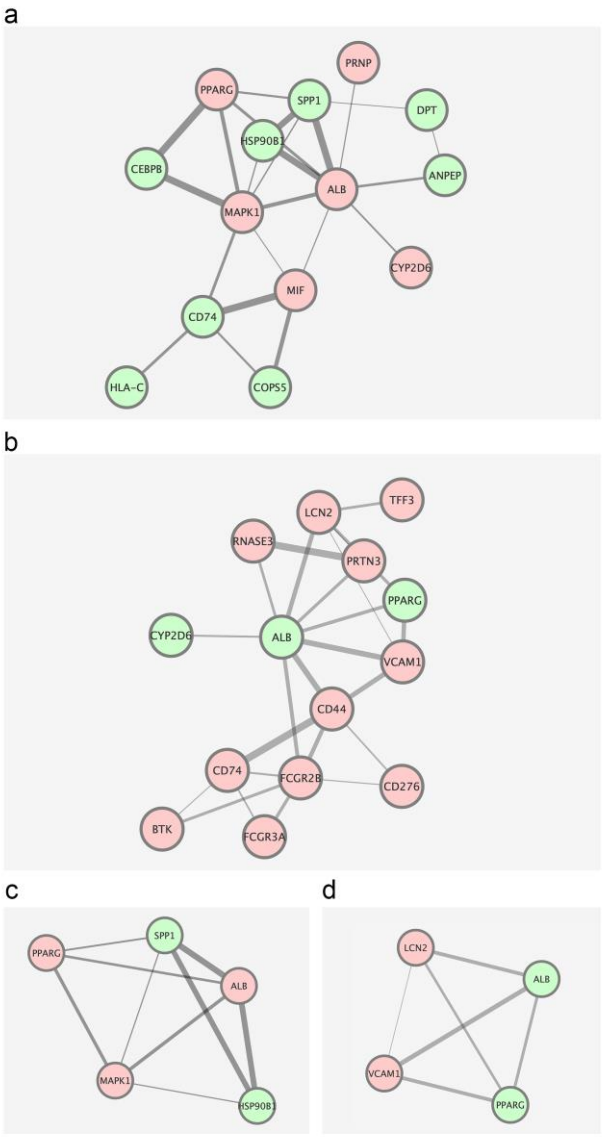

Fig. 16 PPI network and highly connected modules of integrated genes. **a, b** PPI network of hypothyroidism and hyperthyroidism. **c, d** Modules from the PPI network in

hypothyroidism and hyperthyroidism group generated by the MCODE algorithm in Cytoscape. Red indicates relative upregulated genes and green indicates relative downregulated genes. The size of the edges represents the strength of the interactions based on the combined score.

3.2.3 Discussion

Given the increasing use of immune checkpoint inhibitors in clinical practice, IRAEs also occur in approximately 60% of patients after ipilimumab administration (Barroso-Sousa et al., 2018). The adverse effects potentially involve every organ system, but the gastrointestinal tract, skin, liver, and endocrine glands are more commonly affected (Spain et al., 2016). When the combination of CTLA-4 and PD-1 blockades is adopted, the symptoms are more severe and can be fatal in some cases (Khoja et al., 2017; Robert et al., 2015). Even though IRAEs are frequently described, the optimal treatment strategies have not been defined and primarily depend on consensus opinion (Postow et al., 2018).

Autoimmune thyroid dysfunction related to CTLA-4 antibody therapy is one of the common IRAEs clinically. A single-center study reported that approximately 23% of melanoma patients treated with ipilimumab developed different degrees of thyroid abnormalities, including primary or sub-clinical hypothyroidism and hyperthyroidism (Morganstein et al., 2017). It is crucial to discriminate between primary and secondary thyroid dysfunction and exclude pre-existing thyroid disorders for the proper treatment. Thus, the thyroid function of patients before and after anti-CTLA-4 treatment should be assessed routinely. However, despite its importance, scheduled thyroid laboratory evaluation is often complicated and inaccessible in cancer patients. This is due to the fact that both acute illnesses and antitumor therapy can affect triiodothyronine (T3) levels in patients (Kaplan et al., 1982). Furthermore, repeating evaluation and following up of thyroid function is also a burden for both patients and medical resources. Therefore, it is critical to elucidate the molecular mechanism of the autoimmune thyroid dysfunction after anti-CTLA-4 therapy to find effective biological markers for the diagnosis, monitoring, and treatment of these patients.

Here, 22 DEGs of hypothyroidism and 17 DEGs of hyperthyroidism associated with anti-CTLA-4 therapy were identified for functional analysis. Results from GO enrichment analysis suggest that these DEGs are mainly involved in apoptosis, protein

binding, and immune regulation. It should also be noted that MAPK1 is the common gene in all the enriched KEGG pathways in the hypothyroidism group. It is also one of the hub genes identified from the PPI network. MAPK1, also known as mitogen-activated protein kinase 1, is a member of the MAP kinase family and is involved in a wide range of biological processes like cell proliferation and angiogenesis. Thyroid hormone activates MAPK by binding to the hormone receptor αvβ3 integrin expressed on various tumor cells to promote cell proliferation. A study demonstrated that an inhibitory thyroxine (T4) analogue tetraiodothyroacetic acid (tetrac) blocked MAPK activation induced by thyroid hormone and prevented the proliferation of myeloma cells (Cohen et al., 2011).

FCGR2B and FCGR3A are the two common genes enriched in KEGG terms of the hyperthyroid group. FCGR2B, also named CD32, and FCGR3A, also named CD16A, are low-affinity receptors for the Fc region of immunoglobulin gamma (IgG) belonging to the immunoglobulin superfamily and involved in a series of immune response. FCGR2B is the only inhibitory IgG Fc receptor that prevents immune overstimulation and regulates immunologic balance (Wang et al., 2018). FCGR2B expressed on B cells suppresses humoral immunity by restraining their activation and inhibiting B cell-mediated antigen presentation to T cells (Smith and Clatworthy, 2010). Therefore, the dysfunction of FCGR2B affects the susceptibility to several autoimmune diseases. The activating Fc receptor FCGR3A is mainly expressed in NK cells and macrophages, and plays an important role in autoimmune disease (Marrack et al., 2001). A previous study indicated that hypothyroidism due to rabbit immunoglobulins injection was attenuated in mice lacking FCGR3, but not in mice lacking FCGR2B (Rocchi et al., 2007).

By the PPI network construction, functional enrichment analysis of the highly connected modules revealed that genes in the hypothyroidism module were mainly enriched in the KEGG term “PI3K-Akt signaling pathway”. Phosphatidylinositol 3′ -kinase (PI3K) is responsible for the generation of phosphatidylinositol 3,4,5-trisphosphate, a second messenger essential for the translocation of Akt (Protein kinase B). Activation of Akt involves fundamental cellular functions such as cell proliferation and survival. The PI3K-Akt pathway is associated with the development of various diseases such as cancer, diabetes mellitus, and autoimmunity (Osaki et al., 2004). Furthermore, five hub

genes with the highest degree of connectivity were identified separately from the hypothyroidism and hyperthyroidism groups. The top five hub genes associated with hypothyroidism are ALB, MAPK1, SPP1, PPARG, and MIF, whereas the hub genes associated with hyperthyroidism are ALB, FCGR2B, CD44, LCN2, and CD74.

Specifically, the hypothyroidism and hyperthyroidism groups share the same hub gene ALB, also known as albumin. Albumin is a multifunctional plasma protein that is highly abundant in human blood (Farrugia, 2010). The center of Albumin consists of hydrophobic radicals that bind sites for a wide range of compounds, such as the hormone T4. It serves as a critical fast exchange resource of the thyroid hormone to rapidly stabilize T4 level (Schussler, 1990). A total of four binding sites for T4 have been identified on the subdomains IIA, IIIA, and IIIB of human serum albumin (Petitpas et al., 2003). The mutation of residue R218 in its subdomain IIA is related to familial dysalbuminemic hyperthyroxinemia (FDH) which is induced by the increased affinity for thyroxine after conformation change and the further elevated serum T4 levels (Petersen et al., 1994).

SPP1, also named osteopontin, plays a critical role in cell-mediated immunity and immunoglobulin production by B cells (Ashkar et al., 2000; Lampe et al., 1991). It is involved in various autoimmune diseases, including systemic lupus erythematosus, rheumatoid arthritis, and multiple sclerosis (Cheng et al., 2019). It was demonstrated that the SPP1 level was increased in the serum of patients suffering from Graves' disease (Xu et al., 2011).

PPARG encodes a member of the peroxisome proliferator-activated receptor (PPAR) subfamily. There are three known isotypes: PPARα, PPARβ, and PPARγ. PPARγ is primarily expressed in adipose tissue, colon, and immune system and takes part in distinct diseases such as obesity, diabetes, atherosclerosis, and cancer (Kersten et al., 2000). A previous study indicated that the PPARγ agonist rosiglitazone raised the thyroxine hormone levels in circulation, and PPARs and thyroid hormone receptors can crosstalk to influence a series of biological processes (Jatwa et al., 2007; Lu and Cheng, 2010).

MIF is a lymphokine released by macrophages, lymphocytes, and epithelial cells and is involved in a variety of cell-mediated immune response and inflammation. T4 is considered as a potential antagonist of MIF as the binding of T4 suppresses the catalytic

activity of the hydrophobic pocket that is associated with the pro-inflammatory activities of MIF. In patients with active antineutrophil cytoplasmic antibody (ANCA)-associated vasculitis (AAV), an increase in MIF was detected with a decreased fT3 level (Wendt et al., 2013). It is noteworthy that MIF binds to its natural receptor CD74, a type II transmembrane protein, to initiate downstream inflammatory signals. The recruitment of CD44, a transmembrane glycoprotein with tyrosine kinase activity, is necessary for the following activation of SRC family non-receptor tyrosine kinases, which result in the phosphorylation of ERK1 and ERK2 (Grieb et al., 2010; Shi et al., 2006). In addition, a study about Graves' disease (GD) showed that the injection of GD lymphocytes into thyroid tissue transplants increased the expression of CD44 significantly, indicating the important role of CD44 in the pathology of autoimmune thyroid diseases (Jungheim et al., 2001).

LCN2 is a small extracellular protein belonging to the lipocalin family. Besides its transportation function of hydrophobic molecules such as lipids, steroids, and retinoids, LCN2 is also associated with immune modulation, metabolic regulation, and tumorigenesis (Yang and Moses, 2009). LCN2 was indicated to be regulated by the thyroid hormone. A study showed that thyroid hormone receptors bound directly to thyroid hormone response elements that are located between positions -1444 and -1427 of the LCN2 promotor and T3 upregulated the expression of LCN2 in a time- and dose-dependent way (Chung et al., 2015).

In summary, as a relatively common IRAEs, autoimmune thyroid dysfunction after anti-CTLA-4 therapy should be brought to the forefront, especially in the systematic therapeutic regime of malignancies in clinical practice. In the present study, the pivotal role of candidate key genes such as MAPK1 and FCGR2B, and the enriched signaling pathway such as PI3K-Akt pathway in the molecular regulation network of autoimmune thyroid disorders were enriched by functional analysis. Also, the five hub genes, including ALB, MAPK1, SPP1, PPARG, and MIF in hypothyroidism and ALB, FCGR2B, CD44, LCN2, and CD74 in hyperthyroidism, were also highlighted by integrated bioinformatic analysis. The identification of the candidate key genes and signaling pathways provides potential targets for the diagnosis and treatment of autoimmune thyroid dysfunction related to anti-CTLA-4. Nevertheless, further in vitro or in vivo experiments should be performed to verify these findings.

4. Discussion

There has been an increasing number of clinical studies evaluating the antitumor efficacy of CIK cell-based immunotherapy. In one of our reports in 2020, we reviewed a total of 106 clinical trials, including 4,889 patients in over 30 distinct tumor entities treated with CIK cells (Zhang and Schmidt-Wolf, 2020). Mild adverse effects and reduced graft-versus-host disease (GVHD) potential were observed in most of the studies. Besides, there are nine studies reporting a significantly increased 5-year survival rate, and a quarter of the studies demonstrated improved mFPS and mOS. CIK cell therapy not only increases short-term antitumor response but also improves long-term clinical benefits. Nevertheless, recurrence and non-responsiveness is still a challenging issue in some cases. Our overall goal here is to investigate if targeting by immune checkpoints could promote the antitumor response of CIK/DC-CIK cells (Study 1). We also discussed autoimmune thyroid dysfunction, an immune-related adverse event after immune checkpoint blockade by bioinformatic analysis (Study 2).

In study 1, we chose two immune checkpoints CD40 and CTLA-4 as the targets to improve the antitumor response of DC-CIK cells. CD40/CD40L represents one of the most important stimulatory immune checkpoints and has an extensive effect on both innate and adaptive immune cells (Tang et al., 2021). CTLA-4, a negative regulator of T cell, is the immune checkpoint studied intensely for clinical purposes. Based on the promising clinical results of the combination in metastatic melanoma, we therefore sought to investigate the antitumor effect of anti-CD40 (G28.5) and anti-CTLA-4 (ipilimumab) in RCC (Bajor et al., 2018). Our analysis showed that, a) G28.5 increased the CD3+CD56+ effector cells of CIK cells by promoting the maturation and activation of DCs, b) G28.5 also increased CTLA-4 expression in CIK cells via DCs, but the increase could be hindered by ipilimumab, c) adding ipilimumab was also able to significantly increase the proportion of CD3+CD56+ cells in DC-CIK cells, d) G28.5 predominated over ipilimumab for cytotoxicity, apoptotic effect and IFN-γ secretion of DC-CIK cells against RCC cells. To investigate why CTLA-4 inhibitor ipilimumab showed a very restrictive effect, we studied the role of Tregs in anti-CTLA-4 treatment and compared the population in activated T cells and CIK cells. Our results showed that ipilimumab had no obvious effect on Tregs in CIK cells, which is distinct from that in T cells. This may partially explain why the addition of ipilimumab did not enhance the antitumor response

of DC-CIK cells. Also, we noticed that both G28.5 and ipilimumab significantly reduced the expression of CD28, the counterpart of CTLA-4, in CIK cells. How this decrease in CD28 accounts for the crosstalk between ipilimumab and CIK cells needs further investigation.

The exact mechanisms of CTLA-4 signaling are still under considerable debate. The primary function of CTLA-4 seems to be exerted in two ways, inhibition of helper T cells and enhancement of Treg immunosuppressive activity (Pardoll, 2012). The physiological action of CTLA-4 blockade should be more complex *in vivo* than *in vitro.* A study found that poorly immunogenic tumors did not respond to anti-CTLA-4 as a single agent. Instead, the tumors responded to anti-CTLA-4 combined with a granulocyte-macrophage colony-stimulating factor (GM-CSF)-transduced cellular vaccine (van Elsas et al., 1999). The finding suggested that, in tumors that do not induce substantial endogenous immune responses, the combination of anti-CTLA4 and a vaccine could cause a strong immune response to slow or inhibit tumor growth.

As the anti-CTLA-4 antibody ipilimumab was approved by the US Food and Drug Administration (FDA) for the treatment of advanced melanoma in 2010, CTLA-4 has been considered one of the most promising immune checkpoints to be targeted. CTLA-4 inhibitors are being clinically studied in patients with different tumor entities, such as non-small cell lung cancer, refractory metastatic colorectal cancer, and metastatic renal cell carcinoma (Chung et al., 2010; Horinouchi et al., 2015; Yang et al., 2007). However, the clinical advantages associated with CTLA-4 inhibitors can be offset by the potentially severe immune-related adverse events, such as autoimmune thyroid dysfunction.

Although autoimmune thyroid dysfunction is one of the common IRAEs clinically, studies about its mechanism after anti-CTLA-4 treatment are rare. In study 2, we therefore investigated the candidate genes and signaling pathways involving in autoimmune thyroid dysfunction related to anti-CTLA-4 therapy. Based on the microarray data in GEO database and gene list from text mining, we identified 22 integrated human DEGs in hypothyroidism and 17 DEGs in hyperthyroidism related to anti-CTLA-4 therapy. Functional enrichment analysis of the PPI network revealed that genes in the hypothyroidism module were mainly enriched in the KEGG term “PI3K-Akt signaling pathway”. Activated Akt regulates a variety of physiological processes, including cell survival, cell cycle, and cellular growth. Studies found that PI3K-Akt

signalling pathway plays an important role in resistance of human cancers, as survival signals induced by several receptors are mediated by this pathway (Fresno Vara et al., 2004). Thus, a better understanding of the relationship between autoimmune thyroid dysfunction after anti-CTLA-4 and PI3K-Akt can help to fully exploit the potential targets for diagnosis and management.

To evaluate the interaction between identified DEGs, the top five hub genes were extracted, including ALB, MAPK1, SPP1, PPARG, and MIF associated with hypothyroidism, and ALB, FCGR2B, CD44, LCN2, and CD74 associated with hyperthyroidism. To mention, ALB, also known as albumin, is the common hub gene identified from both the hypothyroidism and hyperthyroidism groups. Albumin is a multifunctional plasma protein highly abundant in human blood (Farrugia, 2010). The center of Albumin are hydrophobic radicals that are binding sites for hormone T4. Albumin serves as a critical fast exchange resource of the thyroid hormone to rapidly stabilize T4 level. It is therefore worthwhile to investigate the function of Albumin in autoimmune thyroid dysfunction.

Altogether, the identification of the candidate key genes and enriched signaling pathways provides potential biomarkers for autoimmune thyroid dysfunction related to anti-CTLA-4 therapy. Revealing the function of enriched molecules and pathways by bioinformatics might contribute to the future diagnosis and management of IRAEs for cancer patients.

5. Abstract

CIK cells are a heterogeneous population of exceptional T lymphocytes with CD3+CD56+ cells as the primary effectors. CIK cells in combination with DCs have exhibited promising clinical effects on patients with RCC as evidenced by several completed or ongoing clinical trials. However, recurrence and non-responsiveness is still a challenging issue in some patients. In order to improve the antitumor response of DC-CIK cells against RCC, we investigated the effect of anti-CD40 and anti-CTLA-4 antibodies on DC-CIK cells against RCC cell lines. Our analysis showed that, a) anti-CD40 antibody (G28.5) increased the CD3+CD56+ effector cells of CIK cells by promoting the maturation and activation of DCs, b) G28.5 also increased CTLA-4 expression in CIK cells via DCs, but the increase could be hindered by the CTLA-4 inhibitor (ipilimumab), c) adding ipilimumab was also able to significantly increase the proportion of CD3+CD56+ cells in DC-CIK cells, d) anti-CD40 antibodies predominated over anti-CTLA-4 antibodies for cytotoxicity, apoptotic effect and IFN-γ secretion of DC-CIK cells against RCC cells, e) after ipilimumab treatment, the population of Tregs in CIK cells remained unaffected, but ipilimumab combined with G28.5 significantly reduced the expression of CD28 in CIK cells. To summarize, we suggest that the agonistic anti-CD40 antibody rather than CTLA-4 inhibitor may improve the antitumor response of DC-CIK cells, particularly in RCC. Alghough the exact mechanisms of CTLA-4 signaling are still under considerable debate, CTLA-4 has been considered one of the most promising immune checkpoints to be targeted clinically. Nevertheless, the clinical advantages associated with CTLA-4 inhibitors can be offset by the potentially severe immune-related adverse events, including autoimmune thyroid dysfunction. So we next investigated the candidate genes and signaling pathways involved in autoimmune thyroid dysfunction related to anti-CTLA-4 therapy. DEGs were extracted from the intersection of genes from GEO datasets and text mining. The functional enrichment was performed by GO annotation and KEGG pathway analysis. PPI network, module enrichment, and hub gene identification were constructed and visualized by STRING and Cytoscape software. A total of 22 and 17 integrated human DEGs in hypothyroidism and hyperthyroidism groups related to anti-CTLA-4 therapy were identified, respectively. Functional enrichment analysis revealed 24 GO terms and 1

KEGG pathway in the hypothyroid group and 21 GO terms and 2 KEGG pathways in the hyperthyroid group. After PPI network construction, the top five hub genes associated with hypothyroidism were extracted, including ALB, MAPK1, SPP1, PPARG, and MIF, whereas genes associated with hyperthyroidism were ALB, FCGR2B, CD44, LCN2, and CD74. The identification of the candidate key genes and enriched signaling pathways provides potential biomarkers for autoimmune thyroid dysfunction related to anti-CTLA-4 therapy for future diagnosis and management. Taken together, our studies about the critical parts of immunotherapy, CIK cells and immune checkpoint blockade, could provide potential approaches to improve the clinical response of cancer patients.

6. List of figures

7. List of tables

Table 1: Differentially expressed human genes identified from the hypothyroid and hyperthyroid samples compared with their normal controls.

a. Hypothyroidism

DEGs	Gene list
Upregulated	*MBD3L5 PIGT MCM10 BAG1 MYO9B SNRPD1 CCDC127 MAN2C1 EXOSC7 USP19 PTDSS2 PTBP1 CDS2 HP1BP3 PPFIBP2 EIF2B2 OLFML1 SLC35B3 EXTL3 HARS CISH MIF GINS1 SESN1 HEMK1 TMEM131 L3MBTL3 GNPTG TRIB3 DNMT3B PTS ZFAND2A C3orf18 ZKSCAN5 ACYP1 MIDN ERAL1 HDC MORC2 TMEM51 ZFAND1 POLE3 GSTT2B THNSL2 ACTR1A GFER PPARG FLOT2 SCUBE3 MRAP PARK7 IMP4 TBCEL LEMD2 FIBP ACAD8 NUP210 RHBDF1 POLDIP2 GGNBP2 NT5C3A RASGRP2 BRD9 IREB2 APLP2 STUB1 EPAS1 ATG2B CHST8 DECR1 RASA3 SHROOM2 UBOX5 DYM C3orf14 SPSB2 RASGRP4 PTTG1IP INPP5K IFT172 C20orf27 PIPOX EIF2AK2 SLC25A28 CLDN9 CNNM2 NEDD4L MAPK1 ITPR1 CUTC RAC1 MT1F OR5AN1 REC8 MIB2 LSM4 CRELD1 ZYX ALKBH7 GTF2F1 DARS AQP9 JAGN1 SLC44A1 OTUD3 TMEM184B COX6B1 STAB1 DCT ADARB1 MAGED2 RENBP ANTKMT PPM1F SLC25A37 ADAM23 PCBP4 RBBP7 ZBTB17 FARS2 GPR1 CEBPE IRF2BP1 AKR7L UPP1 LUC7L DUS4L ACYP2 FGFRL1 UACA KRTCAP3 ATP6V1C2 LYPLA2 CHMP4B SMN2 ATAD3A PLOD3 WFDC2 SAE1 HYAL2 PGLS C19orf44 ZNF330 ANKH FLOT1 IER3 RASSF1 DNTTIP1 OLIG1 CHCHD4 ABCC4 UBAP2 CYP2A7 SERGEF CSGALNACT2 MMP14 SCARF2 MECR INTS4 OVOL2 SAP30L CIRBP CDCA4 TTYH2 RNF6 PXT1 SEMA4B NRM C8orf82 RNPEPL1 DYNLL2 SREBF2 AQP8 ASB1 BLVRB GAMT GALM COMMD6 SCAMP5 OC90 ADSSL1 GCKR GALK1 DDX17 TSTA3 AKAP8L SERPINB1 NR1I3 ACOT1 DENND5B PPEF2 MNAT1 CSNK1G2 NQO1 LRBA ATP5IF1 SGK1 POP4 MGST3 CYP2D6 TMEM38B IPO5 DENND3 HEBP1 TBC1D5 CSTF1 ETHE1 PUS1 CA14 PGS1 APPL1 UGCG DNAJC13 IL11RA SLC25A19 UBXN6 EIF6 PPME1 SERPINA7 PRNP RPL22 CRYL1 GSTM1 GTPBP2 LRTM1 ERP29 PHC2 PSPC1 IL6R CLN3 HEATR1 MRPL38 MRPS34 NIT1 ATOX1 NSMCE1 MRPS9 GTF2H3 CDIPT C1orf198 FBXO6 ISY1 TIAM2 PPP3R1 OR5AP2 CNGA1 NRBP2 PFDN2 C9orf78 NEU2 LMBR1L REEP4 ZNF623 C11orf80 PRKD2 ABHD10 CLEC11A SPON2 NIBAN2 DBP TMEM8A ISOC2 CBR3 TMCO6 RABGEF1 ZFYVE21 CDKN1C LLGL1 SLITRK1 SLC2A2 TIMM50 ACVR2B SH3GLB2 NRBF2 RAB21 MPST*

	PTRH1 CTF1 GARS ZFHX2 OR11H7 VPS37B RDH5 SOAT2 KRT23 SNX17 MSRB2 GPR45 SFXN5 MFGE8 TNNT1 DYNC1H1 PAK4 ZER1 BOLA1 MAEA PIH1D1 HTATIP2 RAP1GAP TBC1D22A ARRDC4 AXIN1 POFUT1 KCNJ3 ABCG8 RSAD1 LRRC59 TXNL4B RETSAT KLF16 CYP4A11 EEF1G ALG9 MVP PI4KA C6orf226 SCAMP2 TRAPPC10 LPL SF3B2 PRRC1 EIF3D PLEKHA4 NUDT19 LRRC46 SNX2 TUT1 MGRN1 WDR13 GPC1 DOCK6 FMO1 ALB BRF2 CTNNAL1 MTSS1 DBNDD2 MTCH1 UBE2E2 UAP1L1 PARD6B APOA4 APEH CSNK1D NRF1 PIP5K1A FFAR3 VAMP2 TCEAL8 PGAM5 SLC6A9 PFN2 RIT1 ABCC3 UGP2 DDHD2 PSMD4 SPG21 ABTB1 DIABLO SLC1A7 FNTB PROX1 RFC5 EPHX1 TMED4 SEMA4A IL4I1 DDIT3 SLC35E3 FBXW5 EDNRA C16orf58 ADHFE1 GIMAP6 ZDHHC7 UBE2E1 PRDX6 SPOP NIPSNAP1 KPNA6 CWF19L2 DIS3L2 KLHL26 UGT1A6 FAM20B INHBE TEX2 SCAMP1 APOA5 GPBP1L1 CMTM4 C18orf21 HPD EIF3I CC2D1A MYLK CPEB3 ZMYM3 ADORA1 GBA SEMA3F PKP4 HCN3 CDC42SE1 TSC22D3 RASL11B STXBP5L CLDN5 DCUN1D4 LSM1 GTF2E1 RGS16 PEX11B FBXO28 BAG4 CYP4F8 PPP1R3C CHRD CUTA
Downregulated	*KLHL7 RGN TSG101 RPS21 VPS26B KIF1B MTMR14 SIDT2 ASNSD1 HUWE1 ARID4A ALDH1B1 TRAPPC6B IL6ST TFF3 ATP5F1D CTSB TRIM56 NKIRAS1 RNASEK SMPDL3A TRAK1 IFT20 STARD10 SKIV2L ADCY9 GPR146 EED ZKSCAN4 SLC25A42 PON3 PMPCB IDI1 DHCR7 CHMP5 YTHDF2 CNOT4 COX6C COPS5 COMT ZNF263 PSMC2 FOS ELOVL3 ACADSB UBL3 CYP7A1 USP4 CHUK RPL18A FNIP1 HAO1 IRF9 DEK CUEDC2 C2CD2L SPAST HSD17B12 PUS10 PPP1R3B NFIC KLB C4A BCAP31 BCL2L13 MRPL36 GNAI2 MEMO1 KRCC1 CRIPT DDT NARS SRPRA SEC11C WDR82 MFHAS1 LMAN1 VAMP8 ANG TUBB6 ZC3H7A LHFPL6 PURB EIF1B AFF1 SLC25A30 GSTK1 TLCD2 PRPF8 DUSP1 TAX1BP1 IFITM2 CYP3A5 RPUSD3 ARPC2 PANK3 PECR TCP1 CRLS1 C1QC SEC24D CALM2 RGS10 ZMAT1 ARL3 MRPL52 PPARD SKP1 CHD7 IGFBP1 GMPS HINT2 ETFA YWHAG CYP2F1 HCFC1 SPCS1 PAIP2 TOMM70 CTSC MDH2 LYVE1 SLC1A2 NSFL1C GDF15 CD74 HMGCR YWHAB IFRD2 ALDH1A1 PCDH1 TM7SF2 ELAVL1 MPND SNX14 PDIA6 PBRM1 DAAM1 U2AF2 COLEC10 SNX1 MRPL43 SCOC HSF2 COLEC11 ABI1 CPB2 SCFD1 MTTP TUSC1 DHRS7 GPC4 NUDCD2 SPP1 AZGP1 PSMD14 PRKD3 HLA-C C8A YTHDF1 EIF4EBP2 CMTM6 C20orf194 C5orf24 PYGL MPV17 SNRPD3 CYP17A1 NPR2 SLC38A4 NPC1 PPIB H2AFY RGP1 SEMA4G PSMD11 COX7A2 DAG1 TXNDC15 PCMTD2 CALD1 PLAC8 SERINC1 RBP4 REXO2 PGRMC1*

RAD23B HAMP ANKRD46 MRPS18C NUCB1 COX11 ERGIC2 DUSP6 DDX1 ZNF292 PRDX5 YIPF2 EDEM2 SERPINA3 CLDND1 UBE2A TMOD3 PAPSS2 CDH1 SEC63 RNF11 GRB14 VAPA SLC66A2 MAD2L2 SNX3 MRPS2 GLRX3 CCNG2 MAGOH KLF15 GJB2 ACBD4 PCK1 ANGPTL3 DDC IRGM ACSL1 UHRF2 S100A13 COMMD1 AGPAT2 ZCCHC17 TFAM ZC3H15 ACTL6A PLS3 KRT8 SAA2 PTCD3 UCHL3 IMMT ABCD3 RRN3 NDUFB4 BCKDHB EMG1 UBFD1 CS SPARC PFN1 NFU1 PPP1CB GLS2 ATXN10 TMEM19 TMEM167B CCNL1 IGFBP2 EXOC7 ESD DPYD AHSA1 EGR1 PMM2 HSP90AB1 ELOVL2 BUD31 TMEM59 DDOST DDX3X RIC8B ALDOB PTPRB HABP2 PLXNB2 DEXI PSMD6 CFDP1 NFIB TOR1B ZFHX3 VDAC2 ID2 STK40 TMCC1 AADAT GSTM3 NDRG2 ZMPSTE24 TSPAN12 DLD MBD1 POLR1B SERPINA12 PCMT1 ATP5F1A EIF3K IFI27L2 GOSR1 CREB3L3 GMCL2 METTL7B TWISTNB TMSB4Y PCYT1A HYOU1 GCLC NDUFA1 KPNA3 CYP20A1 TIMM10 ARNTL PEX7 MCL1 NDUFB9 COX5A DPT PHAX FTSJ3 HMOX1 FLNB GDE1 C5orf34 DNAJB9 SLAIN2 DUSP16 SP1 BMPR1A NDUFB5 SAA4 ZHX2 SH3GLB1 NDUFS3 GNMT DIO1 SH3BGRL2 LGALS13 HADHB NME7 R3HDM2 CEACAM4 CDV3 LPCAT3 CTSZ HACL1 CHMP2A SLC25A25 KMO DUSP23 PRODH ALCAM ZFP36L1 MRPL16 SH3BGRL NOSTRIN ABCB7 TAF13 FNDC3B USP10 RAB5C CUL1 CBR1 PNO1 MRPS35 HMOX2 LY86 PLSCR1 PPM1K KPNB1 APOF COG2 HES6 ATL2 LONP2 PREPL C6 ATP5F1E GLTP DCN NUDT7 LRRC8A AGPAT3 CCT8 FOXQ1 ETFDH ARL8A CCDC25 AASS ITIH2 IRF2BP2 NDST1 SLC9A3R1 ACO1 NDFIP2 POLR2G YME1L1 OSBPL2 DCUN1D5 SNX7 BAAT HIST1H2BE ADAM9 VBP1 MBL2 SLC27A2 FASTKD1 C1GALT1C1 GFM1 TP53INP2 AKR1E2 PPP4R1 ATP2A2 CFB NMD3 PDCD5 B3GALT1 KIF1C RALBP1 PA2G4 ZFYVE1 MINPP1 CRELD2 EHHADH MAP1LC3B2 TSN BCL6 ATP5PB ATF5 NAGLU SUSD4 SEC16B BCAS2 TDO2 ACP6 FAM162A AADAC ELP2 FGFR1OP2 CTSS KPNA1 RASSF3 CCDC6 TOMM7 SLC35B1 SS18 PIGR TGIF1 AVPR1A KNG1 ARCN1 C11orf54 PSME3 ACADL NR2C1 PSMD12 ULK2 RCHY1 EFNA1 CMAS PTPRE TXNDC12 ZBTB43 MON1A GSTP1 MASP1 PTPRD SARDH SERPINC1 CLDN12 SEPHS2 MGST1 AFM IDH2 C15orf61 SRP9 SDHD CHCHD7 RAB7A MCCC1 SLC25A17 MGLL CGN PSMD9 CEBPB TPCN1 CITED2 AK3 ATXN1 OSGIN1 UHRF1BP1L ACY3 CDO1 APOH MRPL22 PAH LMF1 HAL S100A10 HSPA5 SELENBP1 PTGES3 VTI1B HSP90B1 GLUL CPN2 MLYCD ZNF750 UPP2 ATP6V1A PHLDA1 CYP7B1 TCF25 TM7SF3 LSM6 LIMA1 EI24 DAZAP2 LPGAT1 COX7B LARP4 PDPK1 MED28 HSD17B2 ITGB5 CAPRIN1 USP33 ANPEP INHBC

	ST13 HSD17B6 RP9

b. Hyperthyroidism

DEGs	**Gene list**
Upregulated	*HIST1H4J TSKU TFF3 CCL24 TNFAIP2 ALDH3B1 SQLE CD44 CSF2RA MYOM3 STIM2 CRYBB3 C1QC STX1A LRFN3 NSDHL ALOX5AP TLCD2 FZD7 TYROBP TBXAS1 SLC1A3 SLC25A30 RRM2 GPX1 RSPH1 MAD1L1 C1QA FOXO1 VSIG4 C1QB ASB2 TUBB6 ENO1 HK3 HIST1H1C NCAPH FOLR2 ANKS1A PLD4 RNASE3 KIRREL3 LGMN HOPX CD276 PRC1 SDC3 MCM6 CTSC ST3GAL5 PPARD DNAI1 AIF1 HIST1H2AB CFP CALM2 HLA-DMA HIST1H3A ISYNA1 PRTN3 NT5E LAPTM5 SIGLEC1 FGL1 CD74 COL12A1 GDF15 SLC7A8 P2RY6 SLC22A7 SDF2L1 EVL CYP17A1 PLVAP PLAC8 MTHFD2 PSAT1 APCS KCNK1 HYOU1 CHTF18 SSPO PLA2G7 HMOX1 HP CDCA7 KCNK13 LY86 PBK COL15A1 CBR1 HIST1H4I PRKCB CLEC4A TNK2 NNMT VCAM1 SLC25A45 DIO1 TROAP PTGS1 FNDC3B FNDC5 FCGR1A SLC15A3 IDH3A PTGIS EMILIN2 SORT1 B3GALT1 CIB2 MMD2 ZNF467 APOM WAS AURKA CPNE2 NUDT18 COTL1 ACOT11 TOMM40L TUBA1B PLK1 PFKFB4 FIGNL1 SAA2 LCN2 LGALS13 SLAMF9 LYZ CUX2 ANTXR2 FGF21 RAB34 CDCA2 SELPLG FCGR2B A1BG GBP3 REEP5 DCN MGP AXL INCENP SLC13A3 MS4A8 TLE6 SULT1A4 NCKAP1L PCOLCE2 INSIG2 MCM5 GLTP CDKN1A EGR1 CLEC4F PDLIM4 NCF4 ANLN SNX10 CXCL14 CD52 CLDN14 PAQR9 PREPL FCGR3A IFI27L2 MS4A6A SEC61B CD207 WFDC12 NANS PNPLA3 NMRAL1 LPL ADRB2 CKB TMPRSS2 TP53INP2 CYP51A1 LGALS3 CDKN3 S100A9 SPP2 CDC20 SLC41A2 CYBA CD53 PGK1 MVD CLEC7A SOAT1 TRHDE WFIKKN1 PIK3AP1 CYP7B1 BCL3 SLC16A6 FPR2 SNAI3 HSD17B2 ARHGAP24 GNGT2 C19orf67 S100A8 BTK KIF23 KIF2C ITGB1BP1 AATK P2RY13 BMP7 INSC TIMD4 ATXN1 RAD54L*
Downregulated	*MACROD1 MCM10 DQX1 ZNF395 SOX12 CCT6B MARVELD1 TRIB3 ADCY9 VWCE RANBP3L SMARCA2 PDE4C SLC13A4 OAT HDAC11 TCEA3 PPARG LCMT2 TMEM201 PPL SLC25A37 APOL4 C20orf27 SLC44A1 VLDLR COL27A1 GPR135 OLIG1 UPB1 NOX4 MRPS26 PCBP4 CEBPE MRPL18 KRT23 MGST3 AQP8 CABYR BRAP KIFC2 GAL3ST1 IL17RB IGFBP5 LONRF3 CACNA1D ACOT4 ELL3 ACVR2B DOCK6 COL20A1 KRT8 BHLHB9 ADSSL1 KISS1 ADCY6 NPFF ENPP2 EGLN3 SLC6A16 RAP1GAP LIMD2 OCIAD2 CISD1 SLC2A9 ALB ARSA CYP2J2 RNASEH2A RABEP2 ACOT1 BDH2 ADAMTS7 NGEF HOOK2 NR1I3 SPSB4 CHDH HAMP PCCB*

SERPINA7 MAPK15 CYP2D6 SLC2A2 C19orf12 MKNK2 LGALS4 CDKN1C C4orf47 SLC23A3 BUD13 CLCN2 RDH16 FAM13A C12orf43 ETNK2 CCDC57 NFYB ZMYM3 EPHX1 C16orf74 CYP4F2 TMEM25 ABCC3 AQP4 PDK1 SLCO1A2 DEGS1 ADORA1 SLC17A8 RORC ECHDC2 SUCNR1 LINGO4 TOB1 ROBO1 GRIK5 DCLK3 SARDH HSD17B6 INHBE PRSS8 HSD3B2 SORBS3 SPATA2L

Table 2: Detailed human gene list related to anti-CTLA-4 antibodies retrieved from text mining.

	Gene list
Anti-CTLA-4 antibodies related	*LYST LBR IRF6 CD34 IL10 PDCD1 LAD1 PTPRC CFH PTGS2 SAG LAMC2 NPL SOAT1 TNFSF4 TNFSF18 FASLG AGFG1 SELL F5 SELP XCL1 DPT CD247 PTPRN FCGR3B FCGR3A FCGR2A CD48 SLC11A1 MNDA FCRL3 LMNA MUC1 ICOS CTLA4 CD28 ZBTB7B SHC1 CFLAR TCHH RORC HSPE1 HSPD1P1 HSPD1P4 HSPD1P5 HSPD1P6 HSPD1 STAT4 STAT1 HIST2H2BE NEUROD1 CD160 TFRC PHGDH VTCN1 CD2 CD58 SST PTPN22 SSB AP2M1 LAMP3 PSMA5 IFIH1 DPP4 TNFRSF13B VCAM1 IL12A CXCR4 TM4SF1 CCR6 TAGAP IL12RB2 IL23R ESR1 IL1RN IL1B IL1A JUN SUMO4 B3GAT1 SPATA19 IL11 IFNGR1 SRPR IL18RAP SLC4A2 TBPL1 IL1R1 ENPP1 LAIR1 ARG1 CASR CD86 KIR3DL1 AFF3 HSPA8 CD80 CYP2E1 CBL ZAP70 UROD SOCS3 CD200R1 MGAM BTLA MKI67 FYN KLK8 TRAT1 CBLB APOA1 SLC2A1 FOXO3 GRB2 NCAM1 CD8A IL18 FCGRT VAX1 CD300C GNLY IRF5 ATM SLN BAX MMP8 REGL REG1A LILRB1 FLNB FOXP2 TYR TYRL TOR1A PGLYRP1 PPP2R4 F8 SH3GLB2 CTAG1B CTAG1A GAB2 LCK PTPN11 SCD DST XRCC1 GOLGA2 EPB41 LCN2 MPO IL17A CD79A EPO TGFB1 GABRQ DNTT NR0B2 FGF3 VEGFA HSP90B1 CDR1 TCIRG1 RHOA CD40LG MAF CPSF4 FAS TBX21 ACTN4 CDC42P2 CDC42 TLR4 EPCAM OPRL1 KRIT1 CCR5 CCR1 CCR3 CXCR6 PLS3 TXN CPM PADI4 MDM2 DDX41 TSC22D3 IFNG RNF128 TH1L BAD STAT3 PLCB3 STAT5B MEF2A POR BAAT CTNNB1 NODAL CCR8 CCL17 CCL22 LCP2 IQGAP1 LAT2 ANPEP VEGFC BTK CCR7 NFATC2 CEBPB IL12B TNFRSF1B CSF3 TNFRSF8 STAT6 ITK HAVCR2 ERBB2 NOD2 MLC1 CCL25 CXCL10 RCVRN CYP19A1 IFNB1 IFNA1 COPS5 MUC16 CD83 PCSK1 RAB27A RTEL1 HM13 BCL2L1 CDS1 ICAM1 IL7 SMG1 ICAM3 TYK2 HDAC9 APC CA2 VDR TIMP1 SPP1 IL6 BTN3A1 SNCA CD59 ITCH CDR2 IL2RB CD72 GAD2 APBB1IP CD44 IL3 CSF2 EARS2 SLC22A4 SLC22A5 NFKB1 IL5 IL13 IL4 CD82 SYP TNFRSF18 CLTA TNFRSF4 PPARG FOXP3 TSHR TPO HSPA4*

	IL4R RAF1 LEF1 IL9 NR4A1 CREM CD19 LAT SRC ANXA5 EXT1 TNFRSF14 CD276 IL2 IL21 HLA-C INTU NF1 ATAD2 CD14 ALOX5 MAPK3 SERPINA1 CYP2D6 ITGAL IL15 CCL2 CCL11 TNFRSF25 RBP3 CCL1 TG MIF ADA SLA MAPK8 IL2RG MYO9B EOMES TNFRSF9 SDC4 CCL5 CCL15 NR3C2 CCL18 CCL3 CCL4 CD63 MORF4L1 MORF4 ITGAM SILV ITGAX CDK2 JAK3 INSL3 CCR4 GLB1 CXCR3 MS4A2 ACACA IL12RB1 IL16 MS4A1 CD40 CD74 MTOR GUSB IL23A AKT1 GLS2 MTHFR RASGRF2 DHFR DHFRP1 CIITA LIF ACTB ESR2 FCER2 IL8 LYN GATA3 ALB ITGB2 ENAM PFKFB3 VAV1 IL2RA TP53 TNFSF9 MLANA CD68 JAG1 AIRE ICOSLG PDCD1LG2 CTSD CD274 JAK2 PLCB1 FIGF KIT IDO1 CABIN1 FANCB RB1 PRNP ADRA1D TEC TXK AMELX BCR MAPK1 CDKN1B TNFSF11 TRIM21 MBP CXCL16 IL3RA TLR1 KLRK1 KLRC1 KLRD1 EMB NFKBIA CD69 SIRPA EGLN3 CD81 ITGAE PNOC BCL2 INS CD38 RUNX1 CLEC4C ADCY10 GZMB THBS1 HLA-DRB4 IL7R PTPN6 ATN1 TNFRSF10A TNFRSF10B CD4 LAG3 FCGR2B SLC44A4 PSMB9 SMAD7 IRF7 LRPAP1 HBA1 SOD1 HBA2 NEU1 GAPDHL6 GAPDH PRTN3 SETBP1 CD27 TNFRSF1A IRX2 NDN DSG1 TNF RNASE3 DEFB1 ACE THBD TFF3 UCN2

Table 3: GO enrichment analysis associated with common differentially expressed genes of autoimmune thyroid dysfunction and anti-CTLA-4 antibodies.

a. Hypothyroid genes enriched GO terms.

Category	Term	ID	Count	P value
BP	Negative regulation of apoptotic process	GO:0043066	5	0.002207313
BP	Negative regulation of mature B cell apoptotic process	GO:0002906	2	0.004993451
BP	Positive regulation of chemokine (C-X-C motif) ligand 2 production	GO:2000343	2	0.006238098
BP	Regulation of transcription involved in cell fate commitment	GO:0060850	2	0.006238098
BP	Mammary gland epithelial cell proliferation	GO:0033598	2	0.00996315
BP	Regulation of macrophage	GO:0043030	2	0.011201875

	activation			
BP	Negative regulation of DNA damage response, signal transduction by p53 class mediator	GO:0043518	2	0.016142034
BP	Negative regulation of intrinsic apoptotic signaling pathway in response to DNA damage by p53 class mediator	GO:1902166	2	0.016142034
BP	Prostaglandin biosynthetic process	GO:0001516	2	0.017373395
BP	Positive regulation of B cell proliferation	GO:0030890	2	0.047684688
CC	Extracellular exosome	GO:0070062	12	9.01E-05
CC	Perinuclear region of cytoplasm	GO:0048471	5	0.00503401
CC	Endoplasmic reticulum	GO:0005783	5	0.013647179
CC	Golgi apparatus	GO:0005794	5	0.015690594
CC	Extracellular space	GO:0005615	6	0.016428449
CC	Cell surface	GO:0009986	4	0.023360004
CC	MHC class II protein complex	GO:0042613	2	0.025061062
CC	Extracellular region	GO:0005576	6	0.032887842
CC	Integral component of lumenal side of endoplasmic reticulum membrane	GO:0071556	2	0.032908793
CC	Extracellular matrix	GO:0031012	3	0.045072462
MF	Identical protein binding	GO:0042802	7	1.70E-04
MF	Drug binding	GO:0008144	3	0.003606113
MF	Protein binding	GO:0005515	16	0.031494362
MF	Transcription factor binding	GO:0008134	3	0.043909997

b. Hyperthyroid genes enriched GO terms.

Category	Term	ID	Count	P value
BP	Regulation of immune response	GO:0050776	4	5.92E-04
BP	Regulation of transcription involved in cell fate commitment	GO:0060850	2	0.004755668
BP	Macrophage derived foam cell differentiation	GO:0010742	2	0.005704254
BP	Immune response	GO:0006955	4	0.006872
BP	Negative regulation of DNA damage response, signal transduction by p53 class mediator	GO:0043518	2	0.01232066
BP	Negative regulation of intrinsic apoptotic signaling pathway in response to DNA damage by p53 class mediator	GO:1902166	2	0.01232066
BP	Regulation of glucose metabolic process	GO:0010906	2	0.020766825
BP	Cell maturation	GO:0048469	2	0.033770827
CC	Extracellular exosome	GO:0070062	10	1.98E-04
CC	External side of plasma membrane	GO:0009897	4	7.88E-04
CC	Macrophage migration inhibitory factor receptor complex	GO:0035692	2	0.001755204
CC	Extracellular space	GO:0005615	6	0.004800076
CC	Endoplasmic reticulum	GO:0005783	4	0.03362098
CC	Golgi apparatus	GO:0005794	4	0.037363639
MF	Drug binding	GO:0008144	3	0.002304232
MF	Iron ion binding	GO:0005506	3	0.009010387
MF	IgG binding	GO:0019864	2	0.010379714
MF	Identical protein binding	GO:0042802	4	0.031631477
MF	Cytokine receptor activity	GO:0004896	2	0.033595541
MF	RNA polymerase II transcription factor activity, ligand-activated	GO:0004879	2	0.033595541

	sequence-specific DNA binding			
MF	Oxygen binding	GO:0019825	2	0.043647885

Table 4: KEGG pathway analysis of common differentially expressed genes of autoimmune thyroid dysfunction and anti-CTLA-4 antibodies.

Category	Pathway	ID	Gene count	P value	Genes
Hypothyroidism	Tuberculosis	hsa05152	3	0.048909812	MAPK1, CEBPB, CD74
	Thyroid cancer	hsa05216	2	0.057482735	MAPK1, PPARG
	Focal adhesion	hsa04510	3	0.064120305	MAPK1, FLNB, SPP1
	Prion diseases	hsa05020	2	0.0670778	MAPK1, PRNP
Hyperthyroidism	Osteoclast differentiation	hsa04380	4	0.001309393	FCGR2B, PPARG, FCGR3A, BTK
	Tuberculosis	hsa05152	3	0.036680203	FCGR2B, FCGR3A, CD74

Table 5: Top five hub genes identified from the PPI networks.

Hypothyroidism related genes		**Hyperthyroidism related genes**	
Gene	**Node**	**Gene**	**Node**
ALB	8	ALB	8
MAPK1	7	FCGR2B	6
SPP1	5	CD44	5
PPARG	4	LCN2	5
MIF	4	CD74	4

Table 6: Functional enrichment analysis of genes from the highly interconnected modules.

a. Hypothyroidism

Category	Term	ID	Count	P value
BP	Response to stress	GO:0006950	2	0.014453026
BP	Response to estrogen	GO:0043627	2	0.01539526
BP	Receptor-mediated endocytosis	GO:0006898	2	0.043579902
CC	Perinuclear region of cytoplasm	GO:0048471	3	0.006645122
CC	Golgi apparatus	GO:0005794	3	0.012608444
CC	Extracellular exosome	GO:0070062	4	0.012971117
CC	Extracellular region	GO:0005576	3	0.041477897
MF	Identical protein binding	GO:0042802	3	0.011112225
MF	Protein phosphatase binding	GO:0019903	2	0.014845978
MF	Drug binding	GO:0008144	2	0.017888742
KEGG	PI3K-Akt signaling pathway	hsa04151	3	0.007274867
KEGG	Pathways in cancer	hsa05200	3	0.009397898
KEGG	Thyroid cancer	hsa05216	2	0.012595768
KEGG	Prostate cancer	hsa05215	2	0.037894255
KEGG	Estrogen signaling pathway	hsa04915	2	0.042562603
KEGG	Toll-like receptor signaling pathway	hsa04620	2	0.045525493

b. Hyperthyroidism

Category	Term	ID	Count	P value
BP	Response to nutrient	GO:0007584	2	0.013163186
BP	Cellular response to tumor necrosis factor	GO:0071356	2	0.019524915
CC	Golgi apparatus	GO:0005794	3	0.006508414
CC	Extracellular space	GO:0005615	3	0.015572412

MF	Drug binding	GO:0008144	2	0.013446386

8. References

Ashkar S, Weber G F, Panoutsakopoulou V, Sanchirico M E, Jansson M, Zawaideh S, Rittling S R, Denhardt D T, Glimcher M J, and Cantor H. Eta-1 (osteopontin): an early component of type-1 (cell-mediated) immunity. Science 2000; 287(5454): 860-864

Azuma M, Ito D, Yagita H, Okumura K, Phillips J H, Lanier L L, and Somoza C. B70 antigen is a second ligand for CTLA-4 and CD28. Nature 1993; 366(6450): 76-79

Bajor D L, Mick R, Riese M J, Huang A C, Sullivan B, Richman L P, Torigian D A, George S M, Stelekati E, Chen F, Melenhorst J J, Lacey S F, Xu X, Wherry E J, Gangadhar T C, Amaravadi R K, Schuchter L M, and Vonderheide R H. Long-term outcomes of a phase I study of agonist CD40 antibody and CTLA-4 blockade in patients with metastatic melanoma. Oncoimmunology 2018; 7(10): e1468956

Balan S, Saxena M, and Bhardwaj N. Dendritic cell subsets and locations. Int Rev Cell Mol Biol 2019; 348: 1-68

Banchereau J, Bazan F, Blanchard D, Brière F, Galizzi J P, van Kooten C, Liu Y J, Rousset F, and Saeland S. The CD40 antigen and its ligand. Annu Rev Immunol 1994; 12: 881-922

Baran J, Gerner M, Haeussler M, Nenadic G, and Bergman C M. pubmed2ensembl: a resource for mining the biological literature on genes. PLoS One 2011; 6(9): e24716

Barroso-Sousa R, Barry W T, Garrido-Castro A C, Hodi F S, Min L, Krop I E, and Tolaney S M. Incidence of Endocrine Dysfunction Following the Use of Different Immune Checkpoint Inhibitor Regimens: A Systematic Review and Meta-analysis. JAMA Oncol 2018; 4(2): 173-182

Bolstad B. preprocessCore: a collection of pre-processing functions. R package version 1.46. 0. Journal 2019; (Issue):

Bonanno G, Iudicone P, Mariotti A, Procoli A, Pandolfi A, Fioravanti D, Corallo M, Perillo A, Scambia G, Pierelli L, and Rutella S. Thymoglobulin, interferon-γ and interleukin-2 efficiently expand cytokine-induced killer (CIK) cells in clinical-grade cultures. J Transl Med 2010; 8: 129

Braun D A, Bakouny Z, Hirsch L, Flippot R, Van Allen E M, Wu C J, and Choueiri T K. Beyond conventional immune-checkpoint inhibition - novel immunotherapies for renal cell carcinoma. Nat Rev Clin Oncol 2021; 18(4): 199-214

Brunet J F, Denizot F, Luciani M F, Roux-Dosseto M, Suzan M, Mattei M G, and Golstein P. A new member of the immunoglobulin superfamily--CTLA-4. Nature 1987; 328(6127): 267-270

Byun D J, Wolchok J D, Rosenberg L M, and Girotra M. Cancer immunotherapy - immune checkpoint blockade and associated endocrinopathies. Nat Rev Endocrinol 2017; 13(4): 195-207

Capitanio U, and Montorsi F. Renal cancer. Lancet 2016; 387(10021): 894-906

Cappuzzello E, Tosi A, Zanovello P, Sommaggio R, and Rosato A. Retargeting cytokine-induced killer cell activity by CD16 engagement with clinical-grade antibodies. Oncoimmunology 2016; 5(8): e1199311

Chen C L, Pan Q Z, Weng D S, Xie C M, Zhao J J, Chen M S, Peng R Q, Li D D, Wang Y, Tang Y, Wang Q J, Zhang Z L, Zhang X F, Jiang L J, Zhou Z Q, Zhu Q, He J, Liu Y, Zhou F J, and Xia J C. Safety and activity of PD-1 blockade-activated DC-CIK cells in patients with advanced solid tumors. Oncoimmunology 2018; 7(4): e1417721

Cheng C W, Yang S F, Wang Y H, Fang W F, Lin Y C, Tang K T, and Lin J D. Associations of secreted phosphoprotein 1 and B lymphocyte kinase gene polymorphisms with autoimmune thyroid disease. Eur J Clin Invest 2019; 49(3): e13065

Chung I H, Chen C Y, Lin Y H, Chi H C, Huang Y H, Tai P J, Liao C J, Tsai C Y, Lin S L, Wu M H, Chen C Y, and Lin K H. Thyroid hormone-mediated regulation of lipocalin 2 through the Met/FAK pathway in liver cancer. Oncotarget 2015; 6(17): 15050-15064

Chung K Y, Gore I, Fong L, Venook A, Beck S B, Dorazio P, Criscitiello P J, Healey D I, Huang B, Gomez-Navarro J, and Saltz L B. Phase II study of the anti-cytotoxic T-lymphocyte-associated antigen 4 monoclonal antibody, tremelimumab, in patients with refractory metastatic colorectal cancer. J Clin Oncol 2010; 28(21): 3485-3490

Clough E, and Barrett T. The Gene Expression Omnibus Database. Methods Mol Biol 2016; 1418: 93-110

Cohen K, Ellis M, Khoury S, Davis P J, Hercbergs A, and Ashur-Fabian O. Thyroid hormone is a MAPK-dependent growth factor for human myeloma cells acting via αvβ3 integrin. Mol Cancer Res 2011; 9(10): 1385-1394

Coppin C, Kollmannsberger C, Le L, Porzsolt F, and Wilt T J. Targeted therapy for advanced renal cell cancer (RCC): a Cochrane systematic review of published randomised trials. BJU Int 2011; 108(10): 1556-1563

Darling S M, and Abbott C M. Mouse models of human single gene disorders I: Non-transgenic mice. 1992; 14(6): 359-366

Du X, Tang F, Liu M, Su J, Zhang Y, Wu W, Devenport M, Lazarski C A, Zhang P, Wang X, Ye P, Wang C, Hwang E, Zhu T, Xu T, Zheng P, and Liu Y. A reappraisal of CTLA-4 checkpoint blockade in cancer immunotherapy. Cell Res 2018; 28(4): 416-432

Durinck S, Moreau Y, Kasprzyk A, Davis S, De Moor B, Brazma A, and Huber W. BioMart and Bioconductor: a powerful link between biological databases and microarray data analysis. Bioinformatics 2005; 21(16): 3439-3440

Durinck S, Spellman P T, Birney E, and Huber W. Mapping identifiers for the integration of genomic datasets with the R/Bioconductor package biomaRt. Nat Protoc 2009; 4(8): 1184-1191

Edgar R, Domrachev M, and Lash A E. Gene Expression Omnibus: NCBI gene expression and hybridization array data repository. Nucleic Acids Res 2002; 30(1): 207-210

Egen J G, and Allison J P. Cytotoxic T lymphocyte antigen-4 accumulation in the immunological synapse is regulated by TCR signal strength. Immunity 2002; 16(1): 23-35

Escudier B, Eisen T, Stadler W M, Szczylik C, Oudard S, Staehler M, Negrier S, Chevreau C, Desai A A, Rolland F, Demkow T, Hutson T E, Gore M, Anderson S, Hofilena G, Shan M, Pena C, Lathia C, and Bukowski R M. Sorafenib for treatment of renal cell carcinoma: Final efficacy and safety results of the phase III treatment approaches in renal cancer global evaluation trial. J Clin Oncol 2009; 27(20): 3312-3318

Fallarino F, Grohmann U, Vacca C, Bianchi R, Fioretti M C, and Puccetti P. CD40 ligand and CTLA-4 are reciprocally regulated in the Th1 cell proliferative response sustained by CD8(+) dendritic cells. J Immunol 2002; 169(3): 1182-1188

Farrugia A. Albumin usage in clinical medicine: tradition or therapeutic? Transfus Med Rev 2010; 24(1): 53-63

Finke S, Trojaneck B, Lefterova P, Csipai M, Wagner E, Kircheis R, Neubauer A, Huhn D, Wittig B, and Schmidt-Wolf I G. Increase of proliferation rate and enhancement of antitumor cytotoxicity of expanded human CD3+ CD56+ immunologic effector cells by receptor-mediated transfection with the interleukin-7 gene. Gene Ther 1998; 5(1): 31-39

Freeman G J, Gribben J G, Boussiotis V A, Ng J W, Restivo V A, Jr., Lombard L A, Gray G S, and Nadler L M. Cloning of B7-2: a CTLA-4 counter-receptor that costimulates human T cell proliferation. Science 1993; 262(5135): 909-911

Fresno Vara J A, Casado E, de Castro J, Cejas P, Belda-Iniesta C, and González-Barón M. PI3K/Akt signalling pathway and cancer. Cancer Treat Rev 2004; 30(2): 193-204

Grieb G, Merk M, Bernhagen J, and Bucala R. Macrophage migration inhibitory factor (MIF): a promising biomarker. Drug News Perspect 2010; 23(4): 257-264

Gupta V, and Lehal G S. A survey of text mining techniques and applications. 2009; 1(1): 60-76

Hammers H J, Plimack E R, Infante J R, Rini B I, McDermott D F, Ernstoff M, Voss M H, Sharma P, Pal S K, and Razak A R. Expanded cohort results from CheckMate 016: A phase I study of nivolumab in combination with ipilimumab in metastatic renal cell carcinoma (mRCC). Journal 2015; (Issue):

Hathcock K S, Laszlo G, Dickler H B, Bradshaw J, Linsley P, and Hodes R J. Identification of an alternative CTLA-4 ligand costimulatory for T cell activation. Science 1993; 262(5135): 905-907

Heller M J. DNA microarray technology: devices, systems, and applications. Annu Rev Biomed Eng 2002; 4: 129-153

Hodi F S, O'Day S J, McDermott D F, Weber R W, Sosman J A, Haanen J B, Gonzalez R, Robert C, Schadendorf D, Hassel J C, Akerley W, van den Eertwegh A J, Lutzky J, Lorigan P, Vaubel J M, Linette G P, Hogg D, Ottensmeier C H, Lebbé C, Peschel C, Quirt I, Clark J I, Wolchok J D, Weber J S, Tian J, Yellin M J, Nichol G M, Hoos A, and Urba W J. Improved survival with ipilimumab in patients with metastatic melanoma. N Engl J Med 2010; 363(8): 711-723

Horinouchi H, Yamamoto N, Fujiwara Y, Sekine I, Nokihara H, Kubota K, Kanda S, Yagishita S, Wakui H, Kitazono S, Mizugaki H, Tokudome T, and Tamura T. Phase I study of ipilimumab in phased combination with paclitaxel and carboplatin in Japanese patients with non-small-cell lung cancer. Invest New Drugs 2015; 33(4): 881-889

Hsieh J J, Purdue M P, Signoretti S, Swanton C, Albiges L, Schmidinger M, Heng D Y, Larkin J, and Ficarra V. Renal cell carcinoma. Nat Rev Dis Primers 2017; 3: 17009

Hudes G R. Targeting mTOR in renal cell carcinoma. Cancer 2009; 115(10 Suppl): 2313-2320

Hunter T B, Alsarraj M, Gladue R P, Bedian V, and Antonia S J. An agonist antibody specific for CD40 induces dendritic cell maturation and promotes autologous anti-tumour T-cell responses in an in vitro mixed autologous tumour cell/lymph node cell model. Scand J Immunol 2007; 65(5): 479-486

Introna M. CIK as therapeutic agents against tumors. J Autoimmun 2017; 85: 32-44

Ito D, Ogasawara K, Iwabuchi K, Inuyama Y, and Onoé K. Induction of CTL responses by simultaneous administration of liposomal peptide vaccine with anti-CD40 and anti-CTLA-4 mAb. J Immunol 2000; 164(3): 1230-1235

Jamieson A M, Diefenbach A, McMahon C W, Xiong N, Carlyle J R, and Raulet D H. The role of the NKG2D immunoreceptor in immune cell activation and natural killing. Immunity 2002; 17(1): 19-29

Jatwa R, Parmar H S, Panda S, and Kar A. Amelioration of corticosteroid-induced type 2 diabetes mellitus by rosiglitazone is possibly mediated through stimulation of thyroid function and inhibition of tissue lipid peroxidation in mice. Basic Clin Pharmacol Toxicol 2007; 101(3): 177-180

Jungheim K, Caspar G, Usadel K H, and Schumm-Draeger P M. Expression of intracellular adhesion molecule-1 and vascular cell adhesion molecule-1 and homing factor CD44 after engraftment of Graves' lymphocytes in xenotransplanted human thyroid tissue in athymic nude mice. Thyroid 2001; 11(9): 831-837

Kaplan M M, Larsen P R, Crantz F R, Dzau V J, Rossing T H, and Haddow J E. Prevalence of abnormal thyroid function test results in patients with acute medical illnesses. Am J Med 1982; 72(1): 9-16

Keizman D, Gottfried M, Ish-Shalom M, Maimon N, Peer A, Neumann A, Hammers H, Eisenberger M A, Sinibaldi V, Pili R, Hayat H, Kovel S, Sella A, Boursi B, Weitzen R, Mermershtain W, Rouvinov K, Berger R, and Carducci M A. Active smoking may negatively affect response rate, progression-free survival, and overall survival of patients with metastatic renal cell carcinoma treated with sunitinib. Oncologist 2014; 19(1): 51-60

Kersten S, Desvergne B, and Wahli W. Roles of PPARs in health and disease. Nature 2000; 405(6785): 421-424

Khoja L, Day D, Wei-Wu Chen T, Siu L L, and Hansen A R. Tumour- and class-specific patterns of immune-related adverse events of immune checkpoint inhibitors: a systematic review. Ann Oncol 2017; 28(10): 2377-2385

Kulasingam V, and Diamandis E P. Strategies for discovering novel cancer biomarkers through utilization of emerging technologies. Nat Clin Pract Oncol 2008; 5(10): 588-599

Lampe M A, Patarca R, Iregui M V, and Cantor H. Polyclonal B cell activation by the Eta-1 cytokine and the development of systemic autoimmune disease. J Immunol 1991; 147(9): 2902-2906

Lin S, Lin Y, Nery J R, Urich M A, Breschi A, Davis C A, Dobin A, Zaleski C, Beer M A, Chapman W C, Gingeras T R, Ecker J R, and Snyder M P. Comparison of the transcriptional landscapes between human and mouse tissues. Proc Natl Acad Sci U S A 2014; 111(48): 17224-17229

Linn Y C, Lau L C, and Hui K M. Generation of cytokine-induced killer cells from leukaemic samples with in vitro cytotoxicity against autologous and allogeneic leukaemic blasts. Br J Haematol 2002; 116(1): 78-86

Linn Y C, Lau S K, Liu B H, Ng L H, Yong H X, and Hui K M. Characterization of the recognition and functional heterogeneity exhibited by cytokine-induced killer cell subsets against acute myeloid leukaemia target cell. Immunology 2009; 126(3): 423-435

Linsley P S, Bradshaw J, Greene J, Peach R, Bennett K L, and Mittler R S. Intracellular trafficking of CTLA-4 and focal localization towards sites of TCR engagement. Immunity 1996; 4(6): 535-543

Linsley P S, Brady W, Urnes M, Grosmaire L S, Damle N K, and Ledbetter J A. CTLA-4 is a second receptor for the B cell activation antigen B7. J Exp Med 1991; 174(3): 561-569

Linsley P S, Greene J L, Brady W, Bajorath J, Ledbetter J A, and Peach R. Human B7-1 (CD80) and B7-2 (CD86) bind with similar avidities but distinct kinetics to CD28 and CTLA-4 receptors. Immunity 1994; 1(9): 793-801

Ljungberg B, Albiges L, Abu-Ghanem Y, Bedke J, Capitanio U, Dabestani S, Fernández-Pello S, Giles R H, Hofmann F, Hora M, Klatte T, Kuusk T, Lam T B, Marconi L, Powles T, Tahbaz R, Volpe A, and Bex A. European Association of Urology Guidelines on Renal Cell Carcinoma: The 2022 Update. Eur Urol 2022:

Ljungberg B, Albiges L, Abu-Ghanem Y, Bensalah K, Dabestani S, Fernández-Pello S, Giles R H, Hofmann F, Hora M, Kuczyk M A, Kuusk T, Lam T B, Marconi L, Merseburger A S, Powles T, Staehler M, Tahbaz R, Volpe A, and Bex A. European Association of Urology Guidelines on Renal Cell Carcinoma: The 2019 Update. Eur Urol 2019; 75(5): 799-810

Lu C, and Cheng S Y. Thyroid hormone receptors regulate adipogenesis and carcinogenesis via crosstalk signaling with peroxisome proliferator-activated receptors. J Mol Endocrinol 2010; 44(3): 143-154

Lu X, Zhu A, Cai X, Jia Z, Han W, Ma L, Zhou M, Qian K, Cen L, and Chen B. Role of NKG2D in cytokine-induced killer cells against multiple myeloma cells. Cancer Biol Ther 2012; 13(8): 623-629

Maher E R, Neumann H P, and Richard S. von Hippel-Lindau disease: a clinical and scientific review. Eur J Hum Genet 2011; 19(6): 617-623

Marrack P, Kappler J, and Kotzin B L. Autoimmune disease: why and where it occurs. Nat Med 2001; 7(8): 899-905

Massari F, Santoni M, Ciccarese C, Santini D, Alfieri S, Martignoni G, Brunelli M, Piva F, Berardi R, Montironi R, Porta C, Cascinu S, and Tortora G. PD-1 blockade therapy in renal cell carcinoma: current studies and future promises. Cancer Treat Rev 2015; 41(2): 114-121

Merkin J, Russell C, Chen P, and Burge C B. Evolutionary dynamics of gene and isoform regulation in Mammalian tissues. Science 2012; 338(6114): 1593-1599

Min L, Vaidya A, and Becker C. Thyroid autoimmunity and ophthalmopathy related to melanoma biological therapy. Eur J Endocrinol 2011; 164(2): 303-307

Moch H, Amin M B, Berney D M, Compérat E M, Gill A J, Hartmann A, Menon S, Raspollini M R, Rubin M A, Srigley J R, Hoon Tan P, Tickoo S K, Tsuzuki T, Turajlic S, Cree I, and Netto G J. The 2022 World Health Organization Classification of Tumours of the Urinary System and Male Genital Organs-Part A: Renal, Penile, and Testicular Tumours. Eur Urol 2022; 82(5): 458-468

Morganstein D L, Lai Z, Spain L, Diem S, Levine D, Mace C, Gore M, and Larkin J. Thyroid abnormalities following the use of cytotoxic T-lymphocyte antigen-4 and programmed death receptor protein-1 inhibitors in the treatment of melanoma. Clin Endocrinol (Oxf) 2017; 86(4): 614-620

Motzer R J, Escudier B, Oudard S, Hutson T E, Porta C, Bracarda S, Grünwald V, Thompson J A, Figlin R A, Hollaender N, Urbanowitz G, Berg W J, Kay A, Lebwohl D,

and Ravaud A. Efficacy of everolimus in advanced renal cell carcinoma: a double-blind, randomised, placebo-controlled phase III trial. Lancet 2008; 372(9637): 449-456

Motzer R J, Hutson T E, Tomczak P, Michaelson M D, Bukowski R M, Rixe O, Oudard S, Negrier S, Szczylik C, Kim S T, Chen I, Bycott P W, Baum C M, and Figlin R A. Sunitinib versus interferon alfa in metastatic renal-cell carcinoma. N Engl J Med 2007; 356(2): 115-124

Motzer R J, Tannir N M, McDermott D F, Arén Frontera O, Melichar B, Choueiri T K, Plimack E R, Barthélémy P, Porta C, George S, Powles T, Donskov F, Neiman V, Kollmannsberger C K, Salman P, Gurney H, Hawkins R, Ravaud A, Grimm M O, Bracarda S, Barrios C H, Tomita Y, Castellano D, Rini B I, Chen A C, Mekan S, McHenry M B, Wind-Rotolo M, Doan J, Sharma P, Hammers H J, and Escudier B. Nivolumab plus Ipilimumab versus Sunitinib in Advanced Renal-Cell Carcinoma. N Engl J Med 2018; 378(14): 1277-1290

Osaki M, Oshimura M, and Ito H. PI3K-Akt pathway: its functions and alterations in human cancer. Apoptosis 2004; 9(6): 667-676

Padala S A, Barsouk A, Thandra K C, Saginala K, Mohammed A, Vakiti A, Rawla P, and Barsouk A. Epidemiology of Renal Cell Carcinoma. World J Oncol 2020; 11(3): 79-87

Pardoll D M. The blockade of immune checkpoints in cancer immunotherapy. Nat Rev Cancer 2012; 12(4): 252-264

Petersen C E, Scottolini A G, Cody L R, Mandel M, Reimer N, and Bhagavan N V. A point mutation in the human serum albumin gene results in familial dysalbuminaemic hyperthyroxinaemia. J Med Genet 1994; 31(5): 355-359

Petitpas I, Petersen C E, Ha C E, Bhattacharya A A, Zunszain P A, Ghuman J, Bhagavan N V, and Curry S. Structural basis of albumin-thyroxine interactions and familial dysalbuminemic hyperthyroxinemia. Proc Natl Acad Sci U S A 2003; 100(11): 6440-6445

Pievani A, Borleri G, Pende D, Moretta L, Rambaldi A, Golay J, and Introna M. Dual-functional capability of CD3+CD56+ CIK cells, a T-cell subset that acquires NK function and retains TCR-mediated specific cytotoxicity. Blood 2011; 118(12): 3301-3310

Postow M A. Managing immune checkpoint-blocking antibody side effects. Am Soc Clin Oncol Educ Book 2015: 76-83

Postow M A, Sidlow R, and Hellmann M D. Immune-Related Adverse Events Associated with Immune Checkpoint Blockade. N Engl J Med 2018; 378(2): 158-168

Riley J L, Mao M, Kobayashi S, Biery M, Burchard J, Cavet G, Gregson B P, June C H, and Linsley P S. Modulation of TCR-induced transcriptional profiles by ligation of CD28, ICOS, and CTLA-4 receptors. Proc Natl Acad Sci U S A 2002; 99(18): 11790-11795

Rini B I, Campbell S C, and Escudier B. Renal cell carcinoma. Lancet 2009; 373(9669): 1119-1132

Ritchie M E, Phipson B, Wu D, Hu Y, Law C W, Shi W, and Smyth G K. limma powers differential expression analyses for RNA-sequencing and microarray studies. Nucleic Acids Res 2015; 43(7): e47

Robert C, Schachter J, Long G V, Arance A, Grob J J, Mortier L, Daud A, Carlino M S, McNeil C, Lotem M, Larkin J, Lorigan P, Neyns B, Blank C U, Hamid O, Mateus C, Shapira-Frommer R, Kosh M, Zhou H, Ibrahim N, Ebbinghaus S, and Ribas A. Pembrolizumab versus Ipilimumab in Advanced Melanoma. N Engl J Med 2015; 372(26): 2521-2532

Rocchi R, Kimura H, Tzou S C, Suzuki K, Rose N R, Pinchera A, Ladenson P W, and Caturegli P. Toll-like receptor-MyD88 and Fc receptor pathways of mast cells mediate the thyroid dysfunctions observed during nonthyroidal illness. Proc Natl Acad Sci U S A 2007; 104(14): 6019-6024

Rudd C E, Taylor A, and Schneider H. CD28 and CTLA-4 coreceptor expression and signal transduction. Immunol Rev 2009; 229(1): 12-26

Ryder M, Callahan M, Postow M A, Wolchok J, and Fagin J A. Endocrine-related adverse events following ipilimumab in patients with advanced melanoma: a comprehensive retrospective review from a single institution. Endocr Relat Cancer 2014; 21(2): 371-381

Scelo G, and Larose T L. Epidemiology and Risk Factors for Kidney Cancer. J Clin Oncol 2018; 36(36): Jco2018791905

Schmidt-Wolf I G, Lefterova P, Mehta B A, Fernandez L P, Huhn D, Blume K G, Weissman I L, and Negrin R S. Phenotypic characterization and identification of effector cells involved in tumor cell recognition of cytokine-induced killer cells. Exp Hematol 1993; 21(13): 1673-1679

Schmidt-Wolf I G, Negrin R S, Kiem H P, Blume K G, and Weissman I L. Use of a SCID mouse/human lymphoma model to evaluate cytokine-induced killer cells with potent antitumor cell activity. J Exp Med 1991; 174(1): 139-149

Schneider H, Downey J, Smith A, Zinselmeyer B H, Rush C, Brewer J M, Wei B, Hogg N, Garside P, and Rudd C E. Reversal of the TCR stop signal by CTLA-4. Science 2006; 313(5795): 1972-1975

Schneider H, Mandelbrot D A, Greenwald R J, Ng F, Lechler R, Sharpe A H, and Rudd C E. Cutting edge: CTLA-4 (CD152) differentially regulates mitogen-activated protein kinases (extracellular signal-regulated kinase and c-Jun N-terminal kinase) in CD4+ T cells from receptor/ligand-deficient mice. J Immunol 2002; 169(7): 3475-3479

Schreiber R D, Old L J, and Smyth M J. Cancer immunoediting: integrating immunity's roles in cancer suppression and promotion. Science 2011; 331(6024): 1565-1570

Schussler G C. Thyroxine-binding proteins. Thyroid 1990; 1(1): 25-34

Selby M J, Engelhardt J J, Quigley M, Henning K A, Chen T, Srinivasan M, and Korman A J. Anti-CTLA-4 antibodies of IgG2a isotype enhance antitumor activity through reduction of intratumoral regulatory T cells. Cancer Immunol Res 2013; 1(1): 32-42

Sharma A, Reutter H, and Ellinger J. DNA Methylation and Bladder Cancer: Where Genotype does not Predict Phenotype. Curr Genomics 2020; 21(1): 34-36

Shi X, Leng L, Wang T, Wang W, Du X, Li J, McDonald C, Chen Z, Murphy J W, Lolis E, Noble P, Knudson W, and Bucala R. CD44 is the signaling component of the macrophage migration inhibitory factor-CD74 receptor complex. Immunity 2006; 25(4): 595-606

Smith K G, and Clatworthy M R. FcgammaRIIB in autoimmunity and infection: evolutionary and therapeutic implications. Nat Rev Immunol 2010; 10(5): 328-343

Sorensen M R, Holst P J, Steffensen M A, Christensen J P, and Thomsen A R. Adenoviral vaccination combined with CD40 stimulation and CTLA-4 blockage can lead to complete tumor regression in a murine melanoma model. Vaccine 2010; 28(41): 6757-6764

Spain L, Diem S, and Larkin J. Management of toxicities of immune checkpoint inhibitors. Cancer Treat Rev 2016; 44: 51-60

Sung H, Ferlay J, Siegel R L, Laversanne M, Soerjomataram I, Jemal A, and Bray F. Global Cancer Statistics 2020: GLOBOCAN Estimates of Incidence and Mortality Worldwide for 36 Cancers in 185 Countries. CA Cancer J Clin 2021; 71(3): 209-249

Tahbaz R, Schmid M, and Merseburger A S. Prevention of kidney cancer incidence and recurrence: lifestyle, medication and nutrition. Curr Opin Urol 2018; 28(1): 62-79

Tang T, Cheng X, Truong B, Sun L, Yang X, and Wang H. Molecular basis and therapeutic implications of CD40/CD40L immune checkpoint. Pharmacol Ther 2021; 219: 107709

Townsend J P, Cavalieri D, and Hartl D L. Population genetic variation in genome-wide gene expression. Mol Biol Evol 2003; 20(6): 955-963

van Elsas A, Hurwitz A A, and Allison J P. Combination immunotherapy of B16 melanoma using anti-cytotoxic T lymphocyte-associated antigen 4 (CTLA-4) and granulocyte/macrophage colony-stimulating factor (GM-CSF)-producing vaccines induces rejection of subcutaneous and metastatic tumors accompanied by autoimmune depigmentation. J Exp Med 1999; 190(3): 355-366

Vasudev N S, Wilson M, Stewart G D, Adeyoju A, Cartledge J, Kimuli M, Datta S, Hanbury D, Hrouda D, Oades G, Patel P, Soomro N, Sullivan M, Webster J, Selby P J, and Banks R E. Challenges of early renal cancer detection: symptom patterns and

incidental diagnosis rate in a multicentre prospective UK cohort of patients presenting with suspected renal cancer. BMJ Open 2020; 10(5): e035938

Verneris M R, Karimi M, Baker J, Jayaswal A, and Negrin R S. Role of NKG2D signaling in the cytotoxicity of activated and expanded CD8+ T cells. Blood 2004; 103(8): 3065-3072

Wang J, Li Z, Xu L, Yang H, and Liu W. Transmembrane domain dependent inhibitory function of FcγRIIB. Protein Cell 2018; 9(12): 1004-1012

Wang Q J, Wang H, Pan K, Li Y Q, Huang L X, Chen S P, He J, Ke M L, Zhao J J, Li J J, Sun J C, Liang X T, Ma H Q, Chen Y B, and Xia J C. Comparative study on anti-tumor immune response of autologous cytokine-induced killer (CIK) cells, dendritic cells-CIK (DC-CIK), and semi-allogeneic DC-CIK. Chin J Cancer 2010; 29(7): 641-648

Wang Z, Zhang Y, Liu Y, Wang L, Zhao L, Yang T, He C, Song Y, and Gao Q. Association of myeloid-derived suppressor cells and efficacy of cytokine-induced killer cell immunotherapy in metastatic renal cell carcinoma patients. J Immunother 2014; 37(1): 43-50

Wendt M, Börjesson O, Avik A, Bratt J, Anderstam B, Qureshi A R, Miller E J, Gunnarsson I, and Bruchfeld A. Macrophage migration inhibitory factor (MIF) and thyroid hormone alterations in antineutrophil cytoplasmic antibody (ANCA)-associated vasculitis (AAV). Mol Med 2013; 19(1): 109-114

Wu X, Sharma A, Oldenburg J, Weiher H, Essler M, Skowasch D, and Schmidt-Wolf I G H. NKG2D Engagement Alone Is Sufficient to Activate Cytokine-Induced Killer Cells While 2B4 Only Provides Limited Coactivation. Front Immunol 2021; 12: 731767

Wu X, Zhang Y, Li Y, and Schmidt-Wolf I G H. Increase of Antitumoral Effects of Cytokine-Induced Killer Cells by Antibody-Mediated Inhibition of MICA Shedding. Cancers (Basel) 2020; 12(7):

Xu L, Ma X, Wang Y, Li X, Qi Y, Cui B, Li X, Ning G, and Wang S. The expression and pathophysiological role of osteopontin in Graves' disease. J Clin Endocrinol Metab 2011; 96(11): E1866-1870

Yang J, and Moses M A. Lipocalin 2: a multifaceted modulator of human cancer. Cell Cycle 2009; 8(15): 2347-2352

Yang J C, Hughes M, Kammula U, Royal R, Sherry R M, Topalian S L, Suri K B, Levy C, Allen T, Mavroukakis S, Lowy I, White D E, and Rosenberg S A. Ipilimumab (anti-CTLA4 antibody) causes regression of metastatic renal cell cancer associated with enteritis and hypophysitis. J Immunother 2007; 30(8): 825-830

Yano H, Thakur A, Tomaszewski E N, Choi M, Deol A, and Lum L G. Ipilimumab augments antitumor activity of bispecific antibody-armed T cells. J Transl Med 2014; 12: 191

Yu S J, Ma C, Heinrich B, Brown Z J, Sandhu M, Zhang Q, Fu Q, Agdashian D, Rosato U, Korangy F, and Greten T F. Targeting the crosstalk between cytokine-induced killer cells and myeloid-derived suppressor cells in hepatocellular carcinoma. J Hepatol 2019; 70(3): 449-457

Zhan H L, Gao X, Pu X Y, Li W, Li Z J, Zhou X F, and Qiu J G. A randomized controlled trial of postoperative tumor lysate-pulsed dendritic cells and cytokine-induced killer cells immunotherapy in patients with localized and locally advanced renal cell carcinoma. Chin Med J (Engl) 2012; 125(21): 3771-3777

Zhang J, Zhu L, Wei J, Liu L, Yin Y, Gu Y, and Shu Y. The effects of cytokine-induced killer cells for the treatment of patients with solid tumors: a clinical retrospective study. J Cancer Res Clin Oncol 2012; 138(6): 1057-1062

Zhang Y, Ellinger J, Ritter M, and Schmidt-Wolf I G H. Clinical Studies Applying Cytokine-Induced Killer Cells for the Treatment of Renal Cell Carcinoma. Cancers (Basel) 2020; 12(9):

Zhang Y, and Schmidt-Wolf I G H. Ten-year update of the international registry on cytokine-induced killer cells in cancer immunotherapy. J Cell Physiol 2020; 235(12): 9291-9303

Zhao X, Zhang Z, Li H, Huang J, Yang S, Xie T, Huang L, Yue D, Xu L, Wang L, Zhang W, and Zhang Y. Cytokine induced killer cell-based immunotherapies in patients with different stages of renal cell carcinoma. Cancer Lett 2015; 362(2): 192-198

Zhu F, Patumcharoenpol P, Zhang C, Yang Y, Chan J, Meechai A, Vongsangnak W, and Shen B. Biomedical text mining and its applications in cancer research. J Biomed Inform 2013; 46(2): 200-211

9. Acknowledgments

I would like to express my gratitude to everyone who has ever helped me and makes this thesis possible.

First of all, I would like to give my heartfelt thanks to my supervisor Prof. Ingo Schmidt-Wolf. Thank you very much for offering me this research position as a PhD student. When I started to write my first paper as a doctoral student, you gave me valuable suggestions for the outline and format of an academic article. It is these suggestions that make it possible for me to publish more articles in our area. Also, you always give me much freedom in research to explore what I am interested in. Thank you for providing support for my ideas. I would also like to thank my second supervisor Prof. Dr. Hans Weiher. You are always so kind to give me helpful suggestions in the annual committee report and in our lab meeting every week. I also would like to thank Prof. Matthias Schmid and Prof. Dirk Skowasch for being members of my doctoral thesis committee.

Moreover, I want to thank my colleague Amit. He always has great ideas for our projects, and he has done lots of work in revising our papers carefully. I would also like to thank Maria, Oliver, and Tanja for what they have done for our lab and for their very kind help in my work and life. I also want to thank Xiaolong, Fangfang, Peng, Yulu, Jingjing, and our other Chinese colleagues. They are always very warm-hearted to help.

Special thanks go to my family. It is the support of my mother that allows me to study in Germany as a doctoral student.